Proton Magnetic Resonance Spectroscopy for Dementia

7

Akihiko Shiino

Abstract

Proton magnetic resonance spectroscopy (MRS) can be used to investigate metabolite changes and shows potential for clinical study and diagnosis of degenerative disorders such as mild cognitive impairment (MCI), Alzheimer's disease (AD), dementia with Lewy bodies (DLB), and frontotemporal dementia (FTD). The common features of those degenerative disorders include a decrease in the concentration of NAA or in the NAA/Cr ratio and increase in the concentration of mIns or in the mIns/Cr ratio. Moreover, these findings tend to be regionally specific to the diseases, for example, to the hippocampus and the posterior cingulate and precuneal cortices in cases of AD, to the occipital lobe in cases of DLB, and to the frontal lobe in cases of FTD. Therefore MRS has potential clinical utility to differentiate those disorders. However, this approach may not be thoroughly established due to the inherent difficulty of quantitative measurement of metabolites, and therefore its utility is still limited to the local institutional level. In this section, we first briefly introduce the basic theory and principal methodologies of MRS, which may be useful to cultivate a better understanding of targeting for clinicians and neuroscientists, and then discuss the clinical uses of MRS in dementia by reviewing the literature.

Keywords

Magnetic resonance spectroscopy • Dementia • Alzheimer's disease • Mild cognitive impairment • Chemical shift

A. Shiino
Division of Biomedical MR Science, Molecular Neuroscience Research Center, Shiga University of Medical Science, Seta Tsukinowa-cyo, Otsu, Shiga 520-2192, Japan
e-mail: shiino@belle.shiga-med.ac.jp

H. Matsuda et al. (eds.), *Neuroimaging Diagnosis for Alzheimer's Disease and Other Dementias*, DOI 10.1007/978-4-431-55133-1_7

7.1 Introduction

Magnetic resonance spectroscopy (MRS) allows noninvasive in vivo measurement of certain metabolites, with a detection threshold of approximately 0.5–1.0 mM. In 1992, Klunk et al. [1] reported that magnitude of decrease of N-acetylaspartate (NAA) correlated with the number of senile plaques and neurofibrillary tangles in postmortem brain samples from Alzheimer's disease (AD) patients. Soon after, the first report on the use of in vivo MRS was published by Shiino et al. [2] showing that the NAA to creatine + phosphocreatine (Cr) ratio was more than 30% lower in demented patients. In addition to decreased NAA levels, Miller et al. reported elevated myoinositol (mIns)-to-Cr ratios in AD patients [3]. At present, NAA is thought to be a marker of neuronal integrity, and an increased level of mIns is thought to indicate some glial response. The findings of decreased NAA and elevated mIns in patients with AD or mild cognitive impairment (MCI) have largely been confirmed in several studies, even in the early stage of the disease. The clinical use of MRS for investigation of patients with cognitive impairment, however, may not be thoroughly established due to inherent difficulty in quantitative measurement of metabolites or multifarious settings of acquisition parameters including the sequence used, voxel size and location, TR/TE setting, and post-processing methods. There are no standardized referable values to which all results can be compared. Therefore the power of MR spectroscopy is still limited to the local institutional level and lacks evidence from large clinical trials. This chapter firstly introduces a brief basic theory and principal methodologies of single-voxel proton MRS, which may be useful to cultivate a better understanding of targeting for clinicians and neuroscientists, and secondly this chapter discusses the clinical uses of MRS in dementia by reviewing the literature.

7.2 Basic Principals of Magnetic Resonance Spectroscopy

MRS has been used to investigate brain neurochemistry. The basic physical principles of proton (^{1}H) MRS are the same as those of MR imaging and can be done with conventional MR imaging machines. MRS is also applicable to other nuclei such as carbon (^{13}C) and phosphorus (^{31}P), as shown in Table 7.1. Since resonance frequency (Larmor frequency, ω_0) varies among nuclei, additional hardware is generally needed for MRS of those nuclei.

The difference between MRS and MRI is that MRS detects the different chemical components within tissues, whereas MRI shows the anatomical architecture. The targeted nuclei have slightly different resonance frequencies due to interactions via the electrons, which induce small magnetic field change μ_e around the nuclei (Fig. 7.1). Because of these small local magnetic field differences, the resonance frequencies of the nuclei will shift known as the "chemical shift." The information produced by MRS is displayed graphically as a spectrum with a chemical shift

Table 7.1 Nuclei commonly used for MRS in vivo

Nucleus	Name	Spin	Frequency (B_0 = 1.5 T)	Inherent sensitivity	Natural abundance (%)
^{1}H	Proton	1/2	63.87	1	99.99
^{7}Li	Lithium	3/2	24.81	0.272	92.58
^{13}C	Carbon	1/2	16.06	0.0159	1.11
^{19}F	Fluorine	1/2	60.08	0.833	100.00
^{23}Na	Sodium	1/2	16.89	0.0925	100.00
^{31}P	Phosphorous	1/2	25.85	0.0663	100.00
^{35}Cl	Chloride	3/2	6.26	0.0047	75.53
^{39}K	Potassium	3/2	2.98	0.00051	93.08

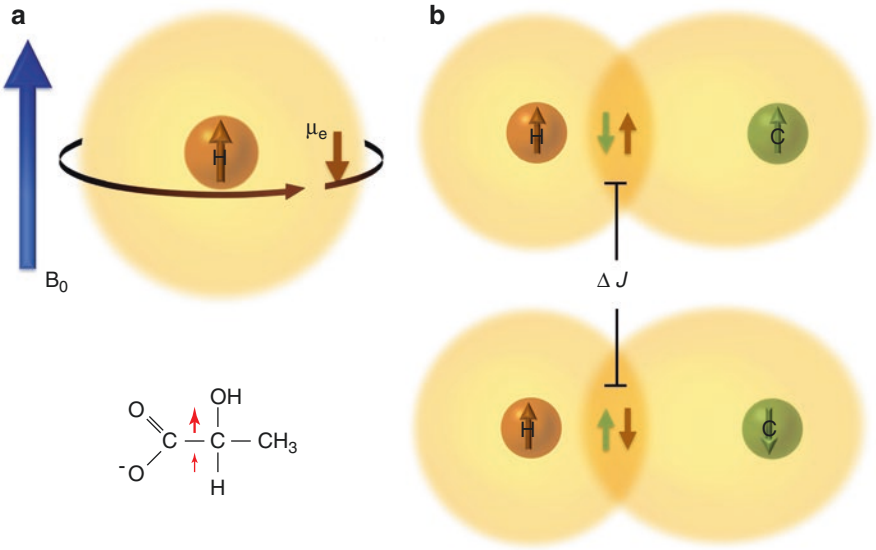

Fig. 7.1 Chemical shift and *J*-coupling. (**a**) Since electrons are negatively charged, the electron cloud shielding a nucleus induces an opposing small magnetic moment μ_e to the applied field. As a result, the nucleus experiences a slightly different magnetic field ($B_0 - \mu_e$), which causes a slight shift of resonance frequency: $B = B_0(1 - \mu_e)$. The oxygen atoms shift the electron density away from the protons leading to reduced electronic shielding; therefore the resonance frequency of the proton nucleus shifts higher. (**b**) The proton resonance is split into a doublet due to scalar coupling with the carbon in which the energy level repeatedly switches between high- and low-spin state. This effect is called *spin-spin coupling* or *J-coupling*

(horizontal) axis in parts per million (ppm) and a signal amplitude (vertical) axis enabling identification of chemical components. Since each signal amplitude or area is proportional to each particular metabolite concentration, one can measure relative or absolute values of concentrations of chemicals.

7.2.1 Chemical Shift

In practice, chemical shift is not expressed in absolute units (such as hertz). This is because the value of chemical shift depends on the applied magnetic field strength; that is, if the magnetic field B_0 is doubled, then the absolute value of the chemical shift will be doubled. Therefore, the chemical shift is measured in relative terms as follows:

$$\text{Chemical shift} = \left(B_{\text{sample}} - B_{\text{reference}}\right) / B_0 = \left(\omega_{\text{sample}} - \omega_{\text{reference}}\right) / \omega_0$$

In proton MRS, tetramethylsilane (TMS), $Si(CH_3)_4$, is traditionally used as universal standard for chemical shift calibration. For example, if the obtained value of the chemical shift between the main peak of *N*-acetylaspartate ($-CH_3$) and TMS ($\omega_{\text{NAA}} - \omega_{\text{TMS}}$) is measured by 1.5 T scanner as 128 Hz, then the chemical shift will be presented as 128/64,000,000 Hz = 2 ppm. Here, the number of 64,000,000 (64 MHz) is the center resonance frequency (ω_0) of protons at 1.5 T. In case of the resonance frequency of the proton in water, the peak appears at 4.7 ppm.

7.2.2 *J*-Coupling and Splitting Pattern

The actual local magnetic field encounters an indirect interaction of neighboring magnetic nuclei (spin-spin splitting) causing perturbation of the electron distribution and splitting of NMR signals. This phenomenon, known as spin-spin coupling or *J*-coupling, provides detailed information on identities of spin-possessing nuclei in a molecule. *J*-coupling can occur between any species of nuclei with spin, in homonuclear (e.g., ^1H–^1H) and heteronuclear (e.g., ^1H–^{13}C) interactions (Fig. 7.1). Peak splitting from *J*-coupling shows the same actual frequency values, whatever the externally applied magnetic field strength, so its value is expressed in "Hz" and not in "ppm." When a species of nucleus is coupled to n equivalent nuclei, its signal splits into an $n + 1$ multiplet, with component amplitude ratios following Pascal's triangle: singlet 1; doublet 1:1; triplet 1:2:1; quartet 1:3:3:1; quintet 1:4:6:4:1; etc. Coupling with additional spin-possessing nuclei causes additional splitting of each component of the multiplet, for example, producing a doublet of doublets.

In lactate (CH_3–CH(OH)–COOH), for example, the methyl groups (CH_3) at 1.31 ppm interact with the methine groups (CH) at 4.10 ppm, and the methyl nucleus signal is split into two equal peaks (a doublet) separated by 6.93 Hz. *J*-coupling also causes phase evolutions that cause peak and baseline distortions that vary with echo time and field strength [4]. This phenomenon is well known as the observation that the lactate doublet has inverted doublet peaks for TE ≈ 143 ms (Fig. 7.2). Since the overlapping within individual metabolites and between other metabolites due to *J*-coupling cancels each other by dephasing effect at longer echo times, metabolites such as γ-aminobutyric acid glutamate and glutamine are hard to measure using long echo times (TE > 50 ms) with in vivo proton spectroscopy [4].

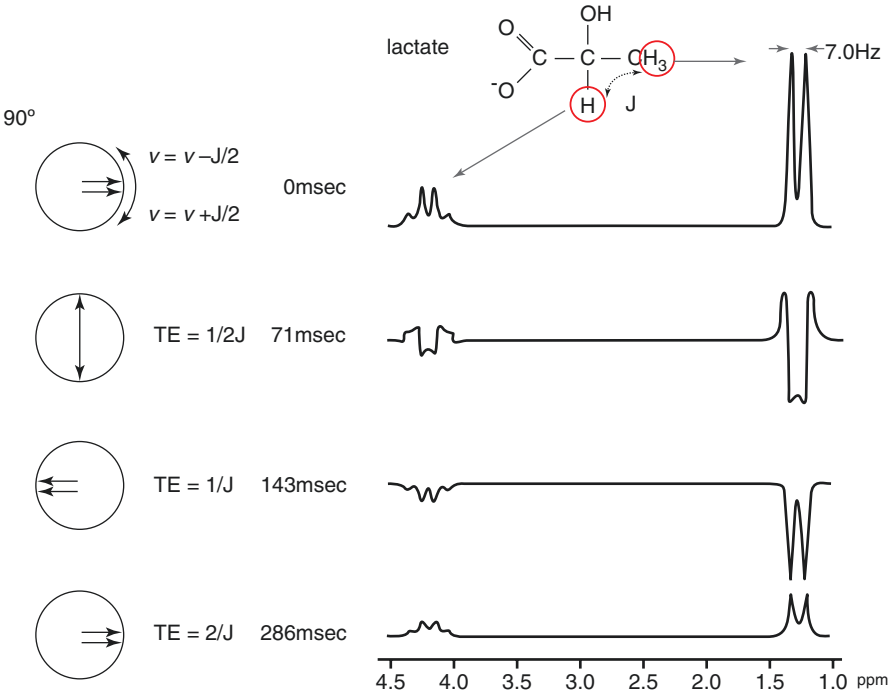

Fig. 7.2 MR spectrum of lactate showing different phase modulations caused by *J*-evolution for different echo times. The proton signal from the methyl group (CH_3) is split into a doublet by the proton of the methine group (CH). On the other hand, the proton signal from the methine group (CH) is split into a quartet with a signal ratio of 1:3:3:1 by the three protons of the methyl group (CH_3). In coupled spin systems, the amplitude and phase of the resonance are modulated and suffer large signal attenuation during T2 decay

7.3 Metabolites Seen by Proton MRS in the Brain

At high magnetic fields of 7 T and above, at least 18 metabolites can be identified noninvasively by MRS [5, 6]. In clinical MR scanners at 1.5 T, the metabolites distinguishable in proton MRS are limited to several metabolites such as choline-containing compounds, creatine + phosphocreatine, glutamine + glutamate, myoinositol, and *N*-acetylaspartate + *N*-acetylaspartylglutamate (NAAG). γ-Aminobutyric acid (GABA) can be measured too by a spectral editing method like MEGA-PRESS in a clinical MR machine at 3.0 T [7].

7.3.1 *N*-Acetylaspartate (NAA)

NAA is an amino acid present in the brain in high concentrations, second in amount to glutamic acid. Interestingly, NAA is found only in the central and peripheral nervous systems and is thought to reflect neuronal density and dysfunction. The

NAA concentrations in the brains of mammals and birds are especially high (up to 10 mM), while in the brains of amphibians, reptiles, and invertebrates, it is much lower [8, 9]. The NAA concentration in the peripheral nervous system and the retina is about 10–20% that of the levels in the central nervous system [10–12]. NAA shows a conspicuous singlet peak at 2.02 from the *N*-acetyl (CH3–CO–NH–) moiety in vivo MRS and has attracted intense interesting from researchers, but little is known about its metabolism and functions. Several functions have been suggested to explain the presence and amount of NAA in the nervous system, including the following:

1. NAA works as an osmoregulator/molecular water pump, removing metabolic water from neurons [13].
2. It is an immediate precursor for NAAG synthesis.
3. It shuttles acetate into oligodendrocytes for myelin synthesis.
4. It is a storage and transport form of acetyl-coenzyme A (acetyl-CoA) in the nervous system that lacks substantial glycogen reserves [14]. Acetyl-CoA cannot cross cell membranes, so it must be converted to citrate in the Krebs cycle for transport to the cytoplasm. NAA may function as an exportable molecule carrying both acetate and aspartate.

NAA is synthesized from L-aspartate and acetyl-CoA by the enzyme aspartate N-aspartate transferase (Asp-NAT) in an oxygen- and ADP-dependent manner. The synthesis increased with age within the first few years of life, and plateaus from age 2 to 20 years, depending on the brain region [15, 16]. In the adult brain, NAA synthesis occurs almost only in neurons [17]. NAA synthesis is coupled to glucose metabolism, and the metabolic relationships can be shown in the following equation [18, 19].

$$40\mathrm{Glc} + 240\mathrm{O_2} = 240\mathrm{CO_2} + 240\mathrm{H_2O} + 1440\mathrm{ATP} + 1\mathrm{NAA} + 0.1\mathrm{NAAG}$$

The time required for NAA synthesis is comparable to that for the brain glycogen synthesis from glucose in the awake rat [20], which takes about 10–14 h [21, 22], and much slower than the synthesis of glutamate, around 1–2 h [23–25]. Furthermore, the NAA synthesis rate in the human brain is in the same range as that found in rat cortex [22]. Therefore, the estimated complete turnover of NAA from glucose is thought to be very slow, taking approximately 70 h [21]. Asp-NAT has not been identified molecularly due to the difficulty of purification, but a recent study indicates that *N*-acetyltransferase 8-like protein (NAT8L) is a strong candidate for Asp-NAT [14, 26]. It has long been believed that NAA is synthesized within mitochondria, but NAT8L is localized to the membrane of endoplasmic reticulum [27]. Glutamate acts as a substrate for NAT8L, with a 50 times lower affinity, and shows competitive inhibition of the aspartate incorporation into NAA [26].

NAA is released to extracellular fluid space and taken up by glial cells via sodium-dependent dicarboxylate (NaDC3) transporters [28]. In oligodendrocytes, NAA is hydrolyzed by aspartoacylase (ASPA) to aspartate and acetate [18], and that acetate is used in lipid synthesis [29] (Fig. 7.3). Deficiency of ASPA causes leukodystrophy, which appears as spongy degeneration of the white matter that is known as Canavan disease [30]. In this case, MRS shows a high concentration of NAA

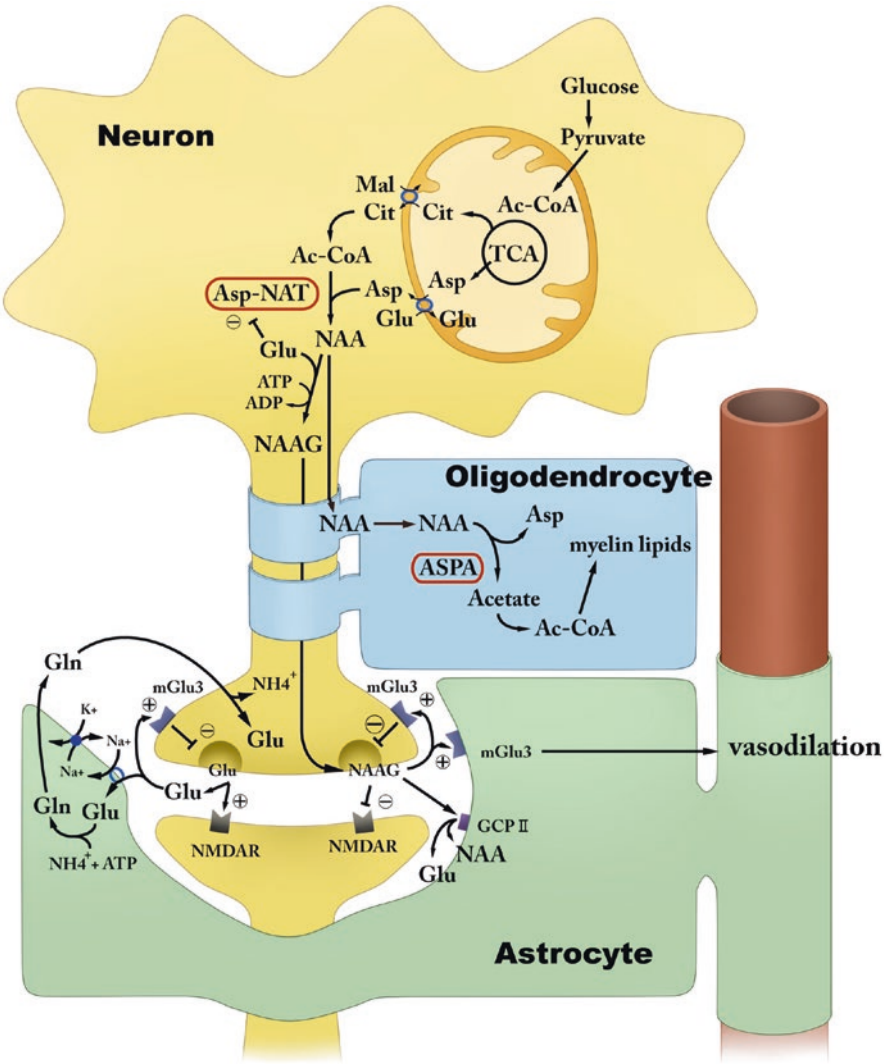

Fig. 7.3 *N*-Acetylaspartate (NAA) and *N*-acetylaspartylglutamate (NAAG) metabolism and function of the brain. Aspartate (Asp) is synthesized in the mitochondria and exported by neuronal AGC1 ARALAR. NAA is synthesized from acetyl-coenzyme A (Ac-CoA) and Asp by aspartate-*N*-acetyltransferase (Asp-NAT), now thought to be a membrane-bound microsomal enzyme. Ac-CoA arises from citrate (Cit) through ATP citrate lyase and is transported into cytoplasm from mitochondria through the citrate carrier. The NAA transporter NaDC3 is primarily expressed in astrocytes and oligodendrocytes and transports NAA into these cells in a Na^+-coupled manner. NAA carries Ac-CoA from neurons to oligodendrocytes for synthesis of myelin lipid. Aspartoacylase (ASPA) cleaves NAA giving rise to acetate and Asp. NAAG is synthesized by NAAG synthetase (NAAGS) in an ATP-dependent reaction. NAAG is released from presynaptic terminals as a neurotransmitter. Released NAAG is degraded into NAA and glutamate extracellularly by GCP-II. NAAG also binds to mGluR3 on presynaptic membranes and inhibits release of neurotransmitters, including glutamate and GABA. NAAG activates mGluR3 on astrocytes, initiating astrocyte Ca^{2+} waves responsible for astrocyte-astrocyte and astrocyte-vascular system signaling and induction of vasodilation and consequent hyperemia in locally activated neurons

which is fairly specific to this disease. Interestingly, there was one reported case of NAA and NAAG deficiency in the brain, possibly due to lack of Asp-NAT [26], and the patient suffered lack of expressive speech, truncal ataxia, seizures, mental retardation, and microcephaly [31–33].

7.3.2 *N*-Acetylaspartylglutamate (NAAG)

NAAG is the most abundant dipeptide of the brain and is synthesized by NAAG synthetase catalyzing the ATP-dependent condensation of NAA and glutamate [34]. Absolute measurement of NAAG has shown that its concentrations in the brain are approximately 0.6–1.5 mM in gray matter and 1.5–2.7 mM in white matter. NAAG is released together with glutamate during neuronal depolarization. NAAG activates metabotropic glutamate receptor mGluR3 [35], localized on presynaptic site of neuron terminal and on astrocyte. The presynaptic mGluR3 receptors inhibit release of neurotransmitters, including glutamate and GABA [36–40]. NAAG also acts on NMDAR as a partial antagonist. These negative modulatory effects of NAAG must be important in synaptic plasticity and also in neuronal protection against excessive glutamate release. NAAG activates mGluR3 on astrocytes, initiating astrocyte Ca^{2+} waves responsible for astrocyte-astrocyte and astrocyte-vascular system signaling and induction of vasodilation and consequent hyperemia in locally activated neurons [19]. As NAAG is a signal molecule specifically targeting the astrocytic mGluR3 receptor, its triggering of brain-activation-related focal BOLD response is thought to be stronger than that of glutamate [41] (Fig. 7.3).

NAAG is hydrolyzed into NAA and glutamate by glutamate carboxypeptidase type II (GCP-II) which is also known as prostate-specific membrane antigen (PSMA) or folate hydrolase 1 (FOLH1), and the products are transported into astrocytes and oligodendrocytes. GCP-II inhibitors have been shown to reduce brain glutamate resulting in neuronal protection in preclinical models of stroke, amyotrophic lateral sclerosis, and neuropathic pain [42].

7.3.3 Creatine and Phosphocreatine (Cr)

Creatine and phosphocreatine (PCr) are abundant in metabolically active tissues such as the muscle, heart, and brain. PCr anaerobically donates a phosphate group to ADP to form ATP via creatine kinase during the first few seconds following an intense muscular or neuronal effort, by the well-known pathway as follows:

$$\mathrm{PCr} + \mathrm{ADP} = \mathrm{ATP} + \mathrm{Creatine}$$

Creatine kinase is highly concentrated in the cerebellum, choroid plexus, and hippocampal granular and pyramidal cells [43]. In postmortem examination, brain-type creatine kinase levels were found to be decreased in the patients with AD, especially in the temporal, cingulate, and occipital cortices [44]. Creatine is biosynthesized endogenously by two sequential steps. The first step is guanidinoacetate

synthesis from arginine by L-arginine/glycine amidinotransferase (AGAT) expressed mostly in the kidneys, and the second step is creatine synthesis from guanidinoacetate by guanidinoacetate methyltransferase (GAMT), expressed mostly in the liver. Creatine is imported through the blood-brain barrier by a specific transporter, SLC6A8, also called creatine transporter (CRT), expressed in the microcapillary endothelial cells. CRT is widely expressed in the adult mammalian brain, particularly in regions related to limbic functions [45–47]. In general, half of creatine stores originate from endogenous synthesis, while the other half is supplied from food. However in the brain, CRT is scarce in astrocytes, particularly in their feet lining microcapillary endothelial cells [48]. Thus the transport of creatine from blood to brain seems to be relatively insufficient [49, 50], and the brain depends more on its own creatine synthesis through AGAT and GAMT expression than on external supply from blood [51, 52]. Both AGAT and GAMT are found in all types of brain cells but rarely together in any one cell [48, 53–55], so guanidinoacetate must be moving from cells holding AGAT to cells holding GAMT [52]. However, guanidinoacetate is not transported without CRT, so in case of CRT deficiency, even with AGAT and GAMT expression in the CNS, MRS finds little or no Cr (creatine and PCr) in the brain [56]. GAMT is expressed strongly in oligodendrocytes, moderately in astrocytes, and very weakly in neurons [55], suggesting that the final step of creatine synthesis in the brain predominates in glial cells.

In proton MRS, the singlet peaks at 3.07 and 3.96 ppm arise from the methyl and methylene protons of creatine and PCr, respectively. The resonances of creatine and PCr are very close, but the methylene resonance of creatine at 3.931 ppm and PCr at 3.930 ppm can be separated into two components at magnetic fields of 7.0 T and higher. Total creatine (Cr) level seems to be fairly stable with time unless there is some severe disease, which is why Cr is usually reliable as an internal standard. However, the Cr signal may increase or decrease in disease.

7.3.4 Choline-Containing Compounds (Cho)

There are several types of phospholipids, including phosphatidylcholine (PC), phosphatidylethanolamine (PE), phosphatidylserine (PS), sphingomyelin, phosphatidylinositol, and cardiolipin. Of these, only PS carries a net negative charge. Newly synthesized lipids are incorporated into the plasma membrane, where PC ends up mainly on the external surface, whereas the aminophospholipids, PS and PE, end up mostly on the cytoplasmic [57]. In most eukaryotic membranes, PC and PE make up some 60–85% of the phospholipid fraction, but the relative amounts of other phospholipids vary between species and between cell types [58]. The major pathway of biosynthesis of PC and PE is the cytidine diphosphate (CDP)-choline and CDP-ethanolamine pathway, known as the “Kennedy” pathway (Fig. 7.4). PE is converted to PC by phosphatidylethanolamine *N*-methyltransferase (PEMT), which occurs mostly in the liver in mammals. Phospholipids are hydrolyzed by phospholipases. PC is catabolized into lyso-PC by phospholipase A or into glycerophosphocholine (GPC) by phospholipase

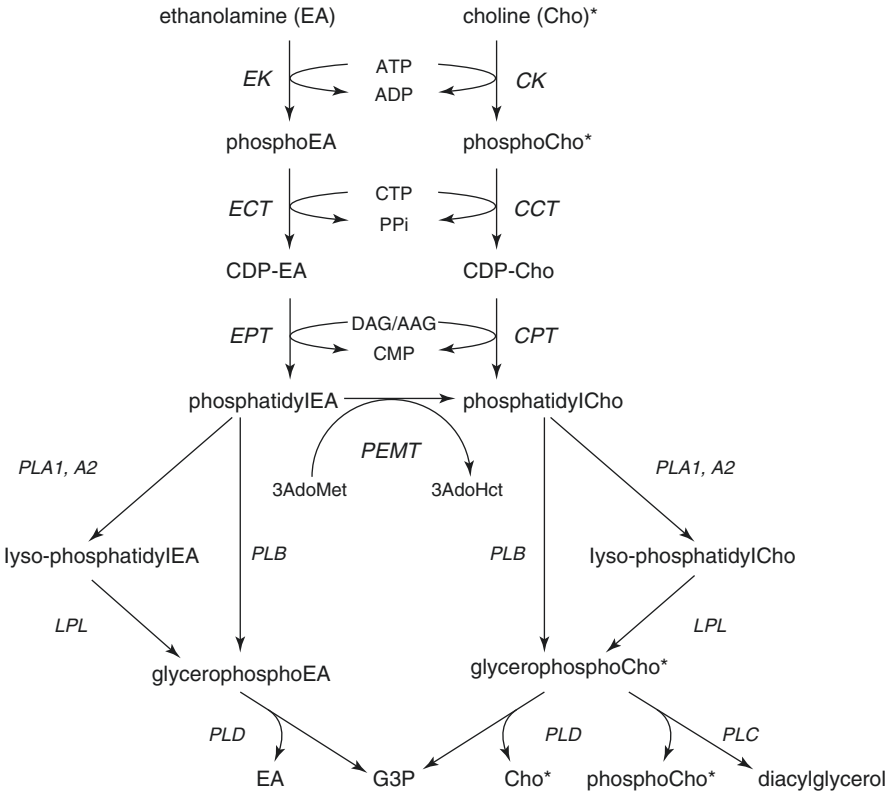

Fig. 7.4 Pathways of glycerophospholipid biosynthesis and catabolism. The glycerophospholipid is synthesized by three enzymatic steps. First, choline kinase (CK) catalyzes the phosphorylation of choline with ATP to form phosphocholine. The second step is the synthesis of high-energy donor CDP-choline, which is rate-limiting of the pathway. This step is catabolized by the phosphocholine cytidylyltransferase (CCT) to synthesize CDP-choline from phosphocholine and CTP. The final step is the synthesis of phosphatidylcholine, which is catabolized by the cholinephosphotransferase (CPT) using CDP-choline and a lipid anchor such as diacylglycerol (DAG) or alkylacylglycerol (AAG) to form phosphatidylcholine [172]. The synthesis of water-soluble glycerophosphocholine (GPC) could involve sequential activity of a phospholipase A (PLA) and a lysophospholipase (LPL) or, alternatively, activity of a single phospholipase B (PLB). GPC is then degraded by hydrolysis to glycerol-3-phosphate (G3P) and choline, catalyzed by phospholipase D (PLD). The synthesis and catabolism of phosphatidylethanolamine is similar to the process of phosphatidylcholine. The MRS-visible choline-containing compounds (*) usually present in cytosol as choline, phosphocholine, and GPC. GPC is produced by cell membrane breakdown, but phosphocholine is produced both in catabolic and anabolic process. *EK* ethanolamine kinase, *ECT* phosphoethanolamine cytidylyltransferase, *EPT* ethanolaminephosphotransferase, *PEMT* phosphatidylethanolamine N-methyltransferase

B. Lyso-PC is rapidly converted to GPC by lysophospholipase (LPL). GPC is then catalyzed into free choline and glycerol-3-phosphate (G3P) by choline phosphodiesterase or phospholipase D (PLD) (Fig. 7.4).

Most of the choline in the brain is located in cell membranes, bound as phospholipids, and this immobile choline is invisible by MRS. Therefore, the Cho peak of MRS reflects water-soluble forms of choline such as phosphorylcholine and GPC. The contribution of free choline seems to be very little because its concentration is usually under detection limit of MRS. The concentration of the total amount of these MRS-visible choline-containing compounds in human brain tissue is approximately 1–2 mM [59–61]. Choline, phosphorylcholine, and GPC show a strong singlet resonance at 3.22 ppm from protons of trimethyl moieties ($-N(CH_3)_3$) at 3.2 ppm, whereby small differences can be observed between 3.5 and 4.3 ppm in multiplet resonances from the remaining CH_2 protons. The concentration of PE in human brain is approximately 0.5–1.0 mN [62], and it can be detected by MRS, as it shows multiplet resonances around 3.1–3.2 and 3.8–4.0 ppm. Possible overlap of resonances from ethanolamine, mIns, glucose, and taurine should be taken into account when using short echo MRS.

The Cho peak is considered as a marker of cellular density and membrane turnover. Elevated Cho signals have been found in tumors, in active demyelination sites, and in inflammation. There is a report that the Cho peak is increased in AD, and in patients with amnestic type MCI (aMCI) who progress to AD, but decreased in patients with aMCI who remain stable [63]. It has also been shown that a higher Cho/Cr ratio in the white matter is associated with an increased risk of developing AD within 4 years [64]. It is reported that soluble Aβ oligomers can open cell channels, letting calcium ions into the cell leading to mitochondrial dysfunction, inflammation, and even cell death [65, 66]. Low concentrations of soluble $A\beta_{1-40}$ or $A\beta_{1-42}$ peptide induce calcium-dependent release of arachidonic acid via inducing PLA_2 activation in a calcium-independent manner [67].

7.3.5 Myoinositol (mIns)

Myoinositol is a major osmolyte released from brain cells, mainly from astrocytes, and also serves as the precursor to phosphatidylinositols. Phosphatidylinositol 4,5-bisphosphate (PIP_2) is the source of the inositol 1,4,5-triphosphate (IP_3), which is a second messenger in signal transduction and lipid signaling. Inositol is a cyclic sugar alcohol consisting of six-carbon rings with six NMR detectable protons and exists in nine possible stereoisomers, of which mIns is the most abundant in human tissue, representing about 90% of total inositol content. The concentration in the brain is normally 4–8 mM, sufficient for MRS sensitivity. NMR of mIns shows a doublet of doublets centered at 3.52 ppm from ^{1}CH and ^{3}CH protons and a triplet at 3.61 ppm from ^{4}CH and ^{6}CH protons. In practice, these proton peaks are seen as a singlet at about 3.57 ppm at 1.5 T. The proton resonances from ^{4}CH and ^{6}CH partially overlap with the glutamate and glutamine multiplet peaks. Since the T2 relaxation time of the ^{4}CH and ^{6}CH protons is short due to their strong coupling, mIns can only be detected at short echo times. The second most concentrated isomer is scyllo-inositol (0.2 mM), which possesses six symmetric protons and evokes a singlet at 3.34 ppm.

Myoinositol is obtained from food and by de novo synthesis. Synthesis and breakdown occur predominantly in the kidneys, so both neurons and glia need to take it in via transporters, sodium/myoinositol cotransporter SMIT1 and SMIT2 and H+/myoinositol cotransporter HMIT. SMIT is expressed in the kidneys and in the brain [68, 69] and is found in both neural and non-neural cells [70]. It is well known that the upregulation of SMIT1 and SMIT2 occurs under hyperosmotic conditions [71–75], whereas no such osmoregulatory function has been reported for HMIT in mammals. SMIT activity is increased by extracellular alkalization, although under physiological conditions, this effect is small. HMIT is activated by extracellular acidification and is close to inactive at pH 7.5 or higher [76]. Since the activity of HMIT is regulated by pH, mIns uptake may induced at any site of low extracellular pH caused by synapse activation or activated glial cells around the synapse [76]. However, the buffering system in the brain is very complicated, and little is known about HMIT. There are many conflicting findings on HMIT, for example, that it is predominately expressed in astrocytes [76] or specifically in neurons [77] and is localized on cell surfaces [78] or in intra-cytosolic membranes [77, 79, 80] and regulating intracellular signaling.

There are several clinical reports of decreased or increased mIns levels of the brain when measured by MRS. It is known that neurodegenerative disorders such as AD, Huntington's disease [81], and spinocerebellar ataxia [82] show increased level of mIns in the affected brain areas. People with Down syndrome show significantly increased mIns concentrations in their parietal [83] and hippocampal [84] regions before neuronal degeneration becomes apparent [85]. Interestingly, the human SMIT gene is located in q22.1 on chromosome 21, and inability to downregulate expression of three copies of the osmoregulatory gene could result in increased flux of mIns [86]. Chronic hyponatremia may cause reduction in mIns [87]; and conversely, chronic hypernatremia increases brain mIns concentration [88]. Ammonia is normally converted to urea in the liver, but in cases of chronic liver dysfunction, accumulated ammonia in the brain is detoxified in astrocytes by conversion to glutamine because of the lack of the urea cycle in the brain. This may increase intracellular osmolarity, and astrocytes may compensate by releasing mIns [89]. Lithium treatment may reduce mIns levels in bipolar patients [90, 91]. Valproate causes 20% reduction of mIns level in mouse frontal cortex [92]. These drugs may inhibit monophosphatase, an enzyme required for inositol recycling and de novo synthesis [93]. However, the proportion of mIns participating the phosphatidylinositol second messenger cycle system appears to be low to affect total brain mIns signal.

Whereas mIns has long been seen as a marker of glial cell proliferation, based on the fact that higher mIns levels are found in cultured astrocytes than in neurons in vitro [94, 95], the true mechanisms of increase or decrease of its concentration remain largely unclear. Brain mIns levels may not always correlate with other molecular markers of gliosis [96–98]. It should be noted that high concentrations of mIns are observed in some types of cultured neurons [99, 100] and that mIns is actively taken up into most types of mature brain cells, including neurons and glia [70]. Therefore the assumption that mIns is a specific glial maker should be treated with caution.

7.3.6 Glutamine and Glutamate (Glx)

In mammalian brains, glutamate is both the main excitatory neurotransmitter and the direct precursor of the inhibitory neurotransmitter γ-aminobutyric acid (GABA). The concentration of glutamate of the brain is about 6–12 mM, with a significant difference between gray and white matter. Under steady-state conditions, two thirds of the glucose oxidation in astrocytes is used for de novo synthesis of glutamate [101], and most astrocytic glutamate is converted to glutamine that is transferred into glutamatergic neurons, completing the glutamate-glutamine cycle. The uptake of synaptic glutamate provides up to 80% of the substrate for glutamine synthesis [102]. Since glutamate transport by excitatory amino acid transporter (EAAT) is coupled to and driven by cotransport of sodium, proton, and potassium ions, any increase in rate of the cycle is matched by increased energy consumption. In this model of glutamate metabolism, glutamate metabolism in the brain is compartmentalized into two pools: a larger neuronal pool comprising about 80% of total glutamate, metabolized with relatively slower turnover time, and a smaller astrocytic pool comprising about 20% of total glutamate, which is rapidly converted to glutamine [103].

NMR of glutamate shows a doublet of doublets centered at 3.75 ppm from the single ^{2}CH methine proton, while the resonances from the other four protons appear as multiplets between 2.04 and 2.35 ppm. Glutamine and glutamate are structurally similar, and their resonances overlap each other. The ^{2}CH methine proton of glutamine shows triplet peak at 3.75 ppm, while the multiplets peaks from the methylene protons are closely resonated between 2.12 and 2.46 ppm. Glutamine has also two amide protons at 6.82 and 7.73 ppm. Unfortunately it is difficult to distinguish between glutamate and glutamine by MRS at low magnetic field strength, so the total amount of glutamate and glutamine is often summed up as Glx. There are minor contributions from glutathione and GABA to this combined signal. Since the concentration of glutamine is almost the same as that of glutamate in the brain [104, 105], the glutamine signal is the major confounder of glutamate quantification. The strong coupling of protons also causes different appearances of spectrum at different echo times and different magnetic field strengths. These factors make their observation and quantification difficult with MRS, although the sum of glutamine and glutamate (Glx) can be quantified with high accuracy. Since the glutamine and glutamate levels can change in opposite directions, the total amount of these metabolites tends to be stable. Most clinical MRS studies can measure only this combined amount, resulting in a reduced sensitivity of Glx as a disease marker. Moreover, about 21% of the total glutamate of the brain is thought to be located in intracellular compartments, in which NMR hardly detects it [106].

7.4 Spectrum Analyses

The area under a peak is proportional to both the number of nuclei per molecule of a metabolite resonating at that frequency and the metabolite concentration to which the nuclei belong. Therefore, quantitative measurement can be done either from the

amplitude of the first data point of the time domain signal, that is, free induction decay (FID), or from the determination of peak areas in the frequency domain after Fourier transformation of FID. Reliable metabolite quantification by MRS is still challenging. One important factor causing systematic error is the baseline correction. The baseline in any MR spectrum is much affected by field inhomogeneities, tissue heterogeneities, and patient movements, all of which may distort the line shape. There have been various proposals to correct these unwanted distortions during signal processing [107–112]. For accurate quantification in short echo MRS of the brain, correction must be made for the contribution of macromolecules to the baseline [113, 114].

A number of advanced techniques based on mathematical models have been developed for analyses of MR spectra. Time domain methods are grossly divided into "black-box" and interactive model methods. HSVD and HSLVD are commonly used black-box methods, so as VARPRO and AMARES are well-known interactive methods. Frequency domain methods can be also divided into nonparametric and parametric methods. Nonparametric quantification is performed by simple integration of the areas under the peaks of interest, but this method cannot disentangle overlapping peaks, and its accuracy is highly dependent on proper phase correction, which is far from trivial [115]. The parametric methods are based on a model function to fit the spectrum represented by LCModel.

VARPRO is a basic program for time domain analysis that uses a simple Osborne's Levenberg-Marquardt algorithm for local optimization. It has been replaced by AMARES, which allows accurate and efficient parameter estimation of MRS signals, using a sophisticated nonlinear fitting in the time domain with prior knowledge about the signal parameters, the model function (Lorentzian, Gaussian, Voigt model), and the type of signal (FID or echo). These methods cannot remove nuisance peaks such as macromolecules, lipids, unsuppressed water, and other unknown signals.

Two other programs, AQSES [109] and QUEST [116], make use of a metabolite basis set, which can be built up from simulated spectra from quantum mechanics such as NMR-SCOPE [117] or GAMMA [118] or from in vitro spectra [119]. AQSES [109] is a program that has been especially developed for short echo MRS. In its framework, VARPRO is modified to enable prior knowledge of upper and lower bounds on the nonlinear parameters, equal phase corrections for each metabolite, and optimize the nonlinear least squares problem. AQSES is freely available as Java open-source software AQSES GUI [109, 118], as a measurement system in the Matlab® graphical user interface SPID [120], and as a plug-in in the jMRUI software package (version 4.1) [121].

The jMRUI software [122] runs in either the time or the frequency domain, using signal processing algorithms such as VARPRO, HLSVD, and AMARES [123]. Basis spectrum fitting in jMRUI is performed by the Quantum ESTimation (QUEST) [116] algorithm, which fits the data to a basis set in the time domain. Both AMARES and QUEST enable handling of macromolecule signals and spectral baselines in a number of ways by truncation or down-weighting of the initial points in FID. jMRUI can also use basic methods such as HSVD or HSLVD that can be applied to remove a residual water signal as preconditioning.

LCModel (Linear Combination of Model) is widely used commercial software [124] that uses frequency domain fitting by a linear combination of individual peak profiles of metabolites. The complexities of metabolite spectra become an advantage for this program, since overlaid peaks from different metabolites can be separated from the information at the peaks of other metabolites. This software is fully automatic (noninteractive) and operator independent, so it is highly suitable for studies across centers. LCModel uses a nearly model-free lineshape function and presumes neither a Lorentzian nor a Gaussian lineshape model. It uses the water signal as an internal reference and integrates with the basis set contained in the software, acquired from the standard phantom. It uses the Levenberg-Marquardt nonlinear fitting algorithm and gives some error assessments of the Cramér-Rao type or the like. Mosconi et al. [125] recently compared those four measurement methods (LCModel, AMARES, QUEST, and AQSES) to see whether they produced different statistical results and found that LCModel worked best in their simulation.

7.5 Quality Control

Reliability of fit can be estimated by Cramér-Rao lower bounds (CRLB) [126]. CRLB gives the minimal possible variance on a fit parameter, so any peak measurement with this value over 20% is usually judged as unreliable. MRS is highly sensitive to inhomogeneities in the magnetic field, so shimming is an important procedure for spectral quality. Shimming reduces field inhomogeneity reading to improve water suppression, signal-to-noise ratio (SNR), and spectral resolution. Since SNR is directly reflected in the CRLB that is more directly linked to confidence limits, CRLB seems to be a better parameter by which to judge the quality of quantified data than mere statements of SNR. Linewidth is defined as the full-width at half-maximum (FWHM) peak height in the frequency domain and also reflected in the CRLB indirectly. Broad linewidth means poor spectral resolution that is critical for model fitting. One should note that CRLB indicates only the quality of the spectral fit and does not necessarily reflect the quality of the original data. CRLB is calculated on the assumption that the fitting model and prior knowledge are correct and that systematic errors are not reflected. Possible sources of systematic error are inaccurate T1 and T2 values for each metabolite, incorrect prior knowledge, difficulties in reference-setting and calibration, ROI position or size, structural mixture of GM/WM/CSF, outer volume signal contamination, and operational mistakes [127]. Fit residual is the difference between the measured signal and the model fit, and ideally this should be flat or only white noise if the model fitting is perfect. Fit residual is usually checked by visual inspection, but numerical estimation has been worked out [128]. In LCModel, residues are used as noise level of SNR. Kreis [127] recommended the following acceptance criteria for MR spectral data as follows: FWHM <0.1 ppm (6.4 Hz at 1.5 T, 12.8 Hz at 3 T), CRLB $\leqq$ 50%, the fitting residual should not contain unexplained features, and the spectra should not contain artifacts. From our experience, it is better to set CRLB acceptance criteria as <15% for clinical use regarding possible dementia.

7.6 Acquisition Parameters and Sequences for MRS

The range of echo time (TE) in brain MRS varies from 18 ms to 288 ms, affecting signal peak height and shape depending on the spin-spin relaxation time (T2) and *J*-coupling of each metabolite. Since diphase and signal loss of protons occurs more rapidly in metabolites with short T2 than long T2, the height of metabolite peaks will change with TE in MRS. For example, in case of the relation between Cr and NAA, since the T2 of Cr is significantly shorter than that of NAA, the peak ratio of NAA/Cr becomes larger in the spectrum obtained from long TE than short TE. Since the T2 relaxation times for Glx and mIns are very short, the peaks of these metabolites cannot be detected at long echo times (Fig. 7.5). This is more obvious in Cho/Cr ratio because T2 for Cho is longer than that for NAA. The T2 values of the metabolites also differ depending on the environment, even in the difference between gray and

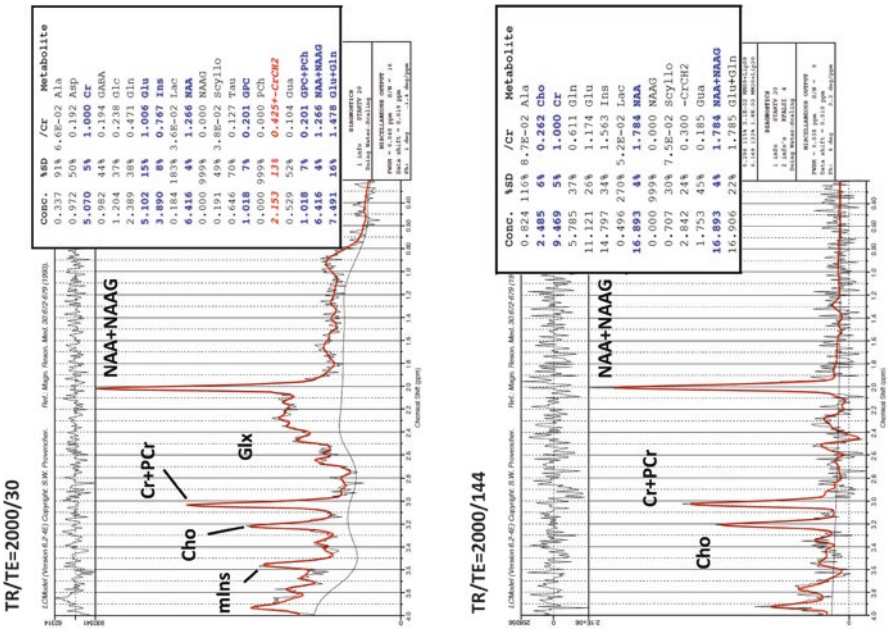

Fig. 7.5 MR spectra of posterior cingulate cortices obtained from normal elderly volunteer. The peak ratio of NAA + NAAG/Cr is 1.266 at echo time = 30 ms, whereas it is 1.784 at echo time = 144. LCModel calculates each metabolite concentration by using tissue water as an internal standard. It should be noted that the default of LCModel for T2 correction of water (T2 = 80 ms) is set at TE = 30 ms, i.e., exp.(−TE/T2) = exp.(−30/80). Therefore if researchers use any TE other than 30 ms, the concentration value of LCModel must be corrected. If TE = 144, then the metabolite concentrations (TE = 144) = (values of LCModel) × exp.(−144/80)/exp.(−30/80) = (values of LCModel) × 0.243. For about NAA + NAAG, it should be 16.893 × 0.243 = 4.105 mM that is too low when compared to the value of 6.416 mM obtained from the results at TE = 30 ms. This is because of the effects of T2 relaxation of NAA and NAAG in vivo, which are uncertain and might differ in each individual. Therefore it is better to use long TR and short TE for quantitative measurement of metabolites to minimize the uncertain effect of T1 and T2 relaxation of the metabolites in vivo

white matter. Longer echo time is sometimes used for lactate identification. Lactate and lipid resonances are overlaid together, but the lipid resonances may decay fully in case of long echo times that facilitate identification of the lactate peak.

Theoretically, metabolite signals are more affected by uncertain T2 when using long TE than short TE that will cause errors in absolute quantification (Fig. 7.5). Therefore using shorter TE seems to be more profitable for absolute quantification. The other advantage of using short TE is to gain higher signal intensity and to enable detection of metabolites with short T2 such as mIns, glutamate, glutamine, GABA, scyllo-inositol, and lipids. On the other hand, this may cause unwanted distortion of the spectrum baseline and superimposition of peaks from metabolites that may lead to errors in both absolute and relative metabolite quantitation. At short TE, multiple resonance peaks between 2.05 and 2.45 ppm from glutamine, glutamate, and GABA partially overlap the NAA peak at 2.01 ppm. Since the information contained in the short TE and long TE spectra are actually complementary, it may be desirable to use short and long TE sequences as far as permitted by total scanning time, patient tolerance, and cost.

There are two major sequences for volume localization in single-volume MRS: stimulated echo acquisition mode (STEAM) and point-resolved spectroscopy (PRESS). STEAM offers advantages for using MRS of very short TE and more effective water suppression than PRESS because the pulses of water suppression can be applied prior to the first slice selective pulse and during the *TM* phase [129]. The advantages of PRESS are that it gives double the signal intensity given by STEAM, it is less disturbed by motion and by diffusion, and it does not suffer from multiple-quantum effects. STEAM has a tendency to acquire a volume larger than the chosen VOI, whereas PRESS has the opposite tendency [130].

The methods for absolute quantification of metabolites are summarized elsewhere [131]. In brief, there are three main methods: internal water reference, external reference, and electrical reference. In the method using internal water reference, the signal from unsuppressed tissue water from the same VOI for MRS is used as internal standard. Researchers need to correct the results by %CSF of the VOI and by T1 and T2 relaxation times of each metabolite and water. The inaccuracy of the method is caused by uncertain tissue water content, uncertain T1 and T2 relaxation times of each metabolite, receiver gain instability, and compartmentation such as gray and white matter in the VOI.

7.7 Clinical Application of MRS for Dementia

Many kinds of disorders cause dementia including neurodegenerative disease, vascular or small vessel disease, brain trauma, hydrocephalus, inflammatory diseases, and metabolic disorders. Of these, neurodegenerative diseases represented by Alzheimer's disease (AD), dementia with Lewy bodies (DLB), and frontotemporal dementia (FTD) are frequently encountered. Recent studies have been disclosing the causes of neurodegenerative dementia at molecular levels, and disease classification is becoming better understood in terms of pathogenesis (Table 7.2).

Table 7.2 Classification of degenerative dementias

Pathology	Disease	Tau	Parkinsonism
Amyloid β	AD	4R + 3R(n)	–
α-Synuclein	DLB	4R + 3R(n)[a]	++
Tau	SD-NFT	4R + 3R(n)	–
	AGD	4R(n,g)	–
	PSP	4R(n,g)	+
	CBD	4R(n,g)	+
	FTDP-17	3R,3R + 4R,4R	+
	Pick	3R(n,g)	–
TDP-43	FTLD-U (PPA, SD)		–
	FTLD-MND(ALS)		–

AD Alzheimer's disease, *DLB* dementia with Lewy bodies, *SD-NFT* senile dementia of the neurofibrillary tangle type, *AGD* argyrophilic grain disease, *PSP* progressive supranuclear palsy, *CBD* corticobasal degeneration, *FTDP-17* frontotemporal dementia with parkinsonism linked to chromosome 17, *Pick* Pick's disease, *FTLD-U* frontotemporal lobar degeneration with ubiquitin, *FTLD-MND* frontotemporal lobar degeneration with motor neuron disease, *PPA* primary progressive aphasia, *SD* semantic dementia, *ALS* amyotrophic lateral sclerosis

4R and 3R indicate 4-repeat tau and 3-repeat tau, respectively. "n" and "g" indicate tau-rerated degeneration of neurons and glia, respectively

[a]In case of multiple system atrophy (MSA), *α*-synucleinopathy occurs both in oligodendrocytes and neurons

The common features seen by MRS in those degenerative disorders are decreased concentrations of NAA or NAA/Cr ratio and increased concentration of mIns or mIns/Cr ratio. Moreover, these findings show a tendency to region specificity, for example, to the hippocampus and the posterior cingulate and precuneal cortices (PCC) in cases of AD, to the occipital lobes of DLB, and to the frontal lobes in case of FTD. Therefore MRS has potential clinical utility to differentiate those disorders. However, searching for such regional distribution anomalies of metabolites may not make MRS the optimal choice in this context, even if using multi-voxel technique. There are many other examinations that can be more adequate for differential diagnosis, such as FDG PET, CBF SPECT, and MRI morphometry. Moreover, new techniques of molecular image targeting pathognomonic biomarkers have been developed, for example, Pittsburg Compound-B (PiB) PET for beta amyloid, PBB3 PET for tau, imaging of dopamine transporter (DAT) or metaiodobenzylguanidine (MIBG) for DLB, and PK11195 PET for microglia. Molecular imaging with target-specific ligands is a promising approach to the early diagnosis of dementia and the evaluation of anti-dementia therapy. Given such alternative diagnostic tools, how can MRS be best exploited for clinical diagnosis of dementia? There is no clear consensus on this. However, there are several clues from previous studies. Firstly, NAA decrease and mIns increase can be identified by MRS before morphometrical change becomes significant. Secondly, MRS provides additional information to clinicians, which improves diagnostic accuracy (Fig. 7.6). MRS is noninvasive, without use of radioactive agents, and is uniquely

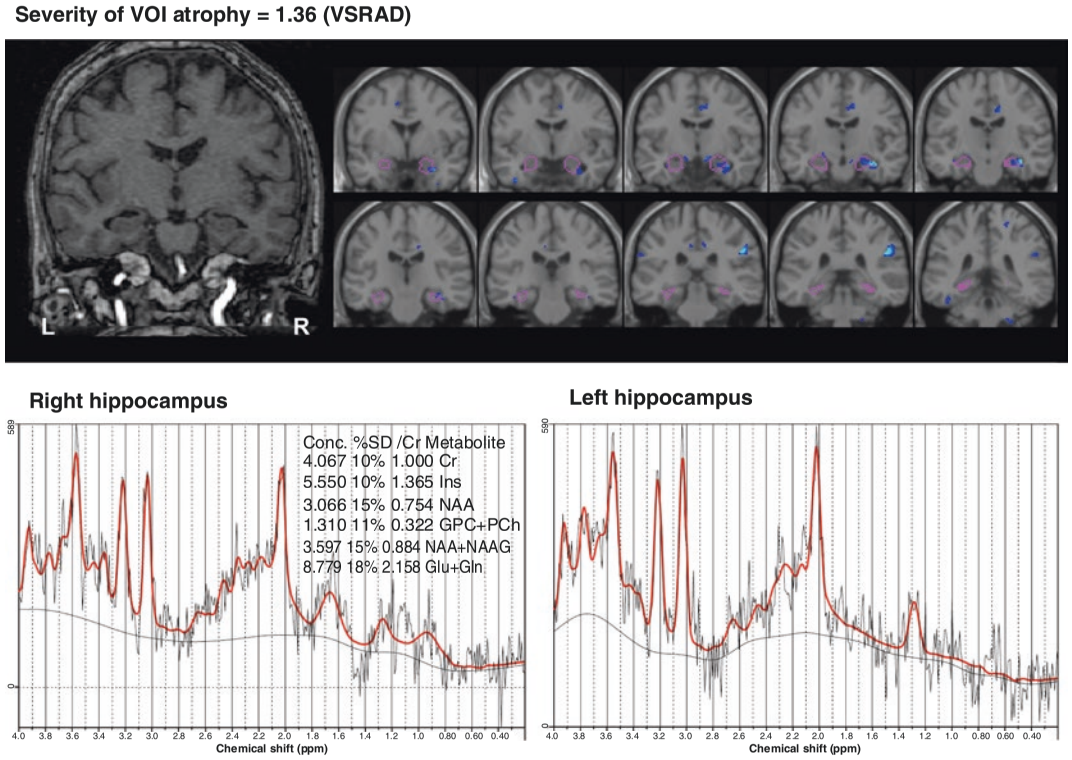

Fig. 7.6 Illustrative case of Alzheimer's disease. A 56-year-old female visited our hospital with her family having a complaint of memory disturbance. She had come to ask the same questions repeatedly following her retirement at 1 year before. At screening, her MMSE score was 28, and CBF SPECT did not show any remarkable abnormality. The hippocampal volume estimated by VSRAD showed slight atrophy (z score = 1.36), which was equivocal as to diagnosis. However, her verbal recognition score in the WMS-R was under 50, and her logical memory II score was 0, indicating deep cognitive impairment. MRS showed significant decrease of NAA + NAAG concentration under 2SD (our institutional range [151]) in her right and left hippocampi and posterior cingulate gyrus. She had no parkinsonian symptoms, and MIBG SPECT showed normal appearance of the heart-to-mediastinum uptake ratio (H/M ratio)

able to provide information on cerebral metabolites that may reflect neuronal or glial activity or transmission. Moreover, MRI and MRS can share the examination time, which is cost-effective and expeditious.

7.7.1 Age-Related Change

Findings on the brain metabolites changes related to normal aging have been inconsistent. Brooks et al. reported that the absolute concentration of NAA decreased significantly with age ($r = -0.42$) with an overall decrease of 12% between the third and seventh decades, whereas any decrease of the concentrations of Cr and Cho was not significant [132]. However, some recent papers showed rather different results. In one study revised from their previous study [133] by adding correction of transverse relaxation time and percentage of cerebrospinal fluid of the voxels centered in the frontal gray and white matter, parietal gray matter, and basal ganglia, the concentration of NAA and Cho showed no significant age-related change, but Cr concentration was significantly increased when measuring frontal white matter [134]. This paper also showed the significant age-related declines in glutamate, especially in the parietal gray matter and basal ganglia [134]. Similar results were reported measuring spectrum of the centrum semiovale, which showed that Cr concentration increased with age ($r = 0.495$, $p < 0.001$), whereas there were no age-related changes in NAA, Cho, and mIns [135]. Another paper [136] showed significant decrease in NAA concentration ($r = -0.36$, $p = 0.007$) and increase in mIns concentration ($r = 0.37$, $p = 0.007$) in the supraventricular white matter. The Cr and Cho concentrations were unchanged with age, but Glx showed U-shaped change with higher concentrations in the young and old subjects [136].

In summary, the age-related changes of metabolite concentrations are not entirely clear, but there seems to be some increase of Cr with age and possible decrease of NAA. Any increase in Cr and mIns may reflect glial cell responses to aging. Researchers need to be aware that metabolite ratios such as the decreased ratio of NAA/Cr that is frequently observed in AD patients do not necessarily mean NAA decrement.

7.7.2 Application to Alzheimer's Disease

Decreased NAA or NAA/Cr ratio has been observed in patients with AD and MCI in medial temporal, posterior cingulate, and parietal cortices. The magnitude of decline has been found to be approximately 10–15% across these brain regions. Several MRS studies have also found an increase in mIns levels by 15–20% in the brain of AD patients. The combination of NAA and mIns measurement may improve the accuracy of discriminating AD patients from normal subjects [137–140]. Decrease of NAA/Cr ratios and increase of mIns/Cr ratios in the PCC correlate with the pathologic severity of AD [141]. NAA/Cr in the medial temporal lobe has been found correlated with Mini-Mental State Examination (MMSE) scores [142]. The

NAA/mIns ratio has also been shown to correlate with MMSE scores and may even be predictive of MMSE decline 12 months later [143]. In a recent study of pathologically confirmed AD patients, reduction of NAA/Cr ratio in the PCC was significantly related to both reduced synaptic vesicle immunoreactivity and accumulation of early intracellular and neuritic hyperphosphorylated tau pathology. Furthermore, elevated mIns/Cr and lower NAA/mIns ratios were found to be related to the accumulation of amyloid-β pathology [144].

The results of MRS studies to distinguish AD patients from normal subjects vary depending on the acquisition parameters of MRS, VOI setting on anatomical regions, measuring single or multi-voxels, and choice of relative or absolute measurements. However, many studies support the clinical usability of MRS as an adjunct diagnostic tool. The overall sensitivity and specificity from the literature for discrimination between AD and normal elderly were 64–94.1% and 72.7–92.3%, respectively. Since the results from these studies have not been validated, the reported values might be somewhat lenient. There is one study showing the results of cross-validation [145]: this study measured hippocampal metabolites in 30 AD and 36 control subjects and compared those findings to the results of MRI-based volumetric analysis. The sensitivity and specificity of MRS alone were 76% and 83%, respectively, somewhat less effective than structural analysis with 93% sensitivity and 86% specificity for the same cohort. Combining the modalities, however, improved the results to 97% sensitivity and 94% specificity. Several other reports confirm the benefits of combining MRS and volumetric MRI for AD diagnosis [140, 146–149]. In a study comparing the diagnostic accuracies of hippocampal volumetry, MRS and diffusion-weighted imaging for discriminating between MCI, AD, and normal elderly subjects [146], the most sensitive tool for distinguishing MCI (79%) and AD (86%) from controls was hippocampal volumetry when specificity was fixed at 80%. For discriminating between AD and MCI, the most sensitive tool was NAA/Cr (67%) measured by MRS of the PCC. Moreover, a combination of these three methods showed better diagnostic sensitivity than any single method for discriminating either AD or MCI from normal. A study of PCC measurement in 25 AD patients, 10 aMCI, and 33 normal volunteers showed an increase of 5.5% for aMCI and of 11.1% for AD in specificity and an increase of 3.7% for aMCI and of 5% for AD in diagnostic accuracy when MRS measures were conjoined with behavioral-functional scales, with a 100% specificity and diagnostic accuracy for distinguishing normal from AD groups [150].

VOI location is also important in clinical use of MRS. There have been many researchers and many variations of VOI settings, and most researches have selected one or a combination of the parietal cortex, PCC, and hippocampus for VOI, those regions being usually involved in AD pathology. Zhu et al. [140] compared 14 AD patients to 22 cognitively normal subjects using short spin-echo (25 ms) MRS imaging (MRSI) with lipid signal nulling by slice selective inversion recovery. AD patients had increased mIns concentrations and mIns/Cr ratios primarily in their parietal gray matter, whereas frontal gray and white matter were spared. In a study of MRSI with long echo time (135 ms) comparing 56 AD patients to 54 cognitively normal subjects [149], NAA concentration was less in AD patients than in healthy

subjects by 21% ($p < 0.0001$) in the medial temporal lobe and by 13–18% ($p < 0.003$) in parietal lobe gray matter but was not changed in gray and white matter of the frontal lobe. MRS of the hippocampus is technically difficult due to its small volume, irregular shape, and location proximity to the skull base or air sinuses which are likely to induce local magnetic field inhomogeneities due to susceptibility difference. However, recently MRS technology has been improving to allow accurate measurements in such regions, and selection of thinner VOIs can reduce susceptibility effects. In a study of single-voxel MRS targeting eight locations of PCC, hippocampus, occipital gray matter, and frontal and parietal white matter in 70 AD patients, 47 aMCI patients, and 52 elderly control subjects, decrease in NAA concentration or increase in mIns concentration was more significant in the hippocampus than in the other regions in both AD and aMCI patients [151].

7.7.3 Application to Mild Cognitive Impairment

MCI is frequently seen as a prodromal stage of dementia and has been a focus for trials to prevent or delay progression to AD. The annual conversion rate of amnestic MCI (aMCI) to AD was approximately 10–15% [152] or 44–64% conversion rate within just 2 years of initial observation [153–155]. However, some aMCI patients do not progress, while some improve over time [156, 157]. In a recent meta-analysis study [158], the adjusted annual conversion rates from MCI to dementia, AD, and VaD were 9.6%, 8.1%, and 1.9%, respectively, diagnosed in specialist centers, and the cumulative proportions who progressed to dementia, to AD, and to VaD were 39.2%, 33.6%, and 6.2%, respectively, which was a low conversion rate than previously thought. This is because MCI is a syndrome representing very heterogeneous disease etiologies. Whereas many MCI patients show AD-type pathology, a substantial number also have non-AD pathology of which cerebrovascular disease is the most common etiology [159]. Therefore an effective test for predicting conversion from MCI to AD would be valuable.

MR spectrum profiles in aMCI patients are generally similar to but milder than those in AD patients [146, 151, 160, 161]. Fortunately a meta-analysis has been done, giving an overview of MRS results (Table 7.3) [162]. As expected, NAA/Cr ratio and NAA concentration were reduced in the PCC and hippocampus of aMCI patients. Effect size was more prominent in NAA concentration than in NAA/Cr ratio. Heterogeneity between studies was lower in NAA concentration ($I^2 = 0.98\%$) than in NAA/Cr ratio ($I^2 = 79.71\%$) when measured in the PCC. The concentration of mIns was increased in PCC, but it was not significant in the hippocampus. It should be noted that the absolute measurements of NAA and mIns in the PCC show significant difference between MCI and normal controls with small variance. Interestingly, Cr concentration is significantly reduced in the hippocampus, but not in the PCC, which may affect the dissociating results of mIns/Cr ratio between the PCC and the hippocampus.

Low concentrations of Cho and Cr in the hippocampus may reflect sparse cellularity or low cellular metabolism in that region. This may be explained by the facts

Table 7.3 Results of the meta-analysis of MCI patients [162]

VOI location	Metabolites	*k*	*n*	ES	CI		*p*	I^2 (%)
Posterior cingulate	**NAA/Cr**	14	798	−0.58	−0.92	−0.24	0.00	79.71
	mIns/Cr	13	774	0.26	−0.04	0.57	0.09	75.25
	Cho/Cr	12	734	0.27	0.00	0.55	0.05	66.71
	NAA/mIns	7	445	−0.76	−1.44	−0.09	0.03	89.83
	NAA	6	383	−0.63	−0.84	−0.42	0.00	0.98
	mIns	6	374	0.39	0.18	0.60	0.00	0
	Cho	6	374	0.09	−0.12	0.30	0.41	6.79
	Cr	5	280	−0.21	−0.45	0.02	0.08	0
Hippocampus	**NAA/Cr**	9	450	−0.43	−0.76	0.09	0.01	59.07
	mIns/Cr	6	218	0.60	0.12	1.09	0.02	63.95
	Cho/Cr	5	182	−0.19	−0.48	0.11	0.21	0
	NAA	5	377	−0.60	−1.03	−0.17	0.01	66.22
	mIns	5	377	−0.03	−0.23	0.31	0.88	21.03
	Cho	5	377	−0.42	−0.70	−0.15	0.00	24.29
	Cr	5	377	−0.40	−0.62	−0.18	0.00	0

k number of studies, *n* total sample size, *ES* effect size for Hedges' g, *CI* confidence intervals, *p* *p*-value, I^2 (%) the percentage of variance in a meta-analysis that is attributable to study heterogeneity (higher value indicates more heterogeneity)
NAA *N*-acetylaspartate + *N*-acetylaspartylglutamate, *mIns* myoinositol, *Cho* choline-containing compounds, *Cr* creatine + phosphocreatine. Minus sign in ES column indicates decrease in MCI compared to controls
Bold characters indicate results significant at $p < 0.05$

that tau pathology generally proceeds earlier in the hippocampus earlier than in the PCC and neuronal loss in the hippocampus must progress substantially to reduce Cho and Cr in MCI patients.

Several longitudinal studies have described differences between converters and non-converters among aMCI patients. The most consistent finding is that converters have lower NAA concentrations and/or lower NAA/Cr ratios than non-converters in several brain regions including the PCC [163, 164], occipital gray matter [164, 165], temporoparietal gray matter [166], and paratrigonal white matter [167]. Unlike those studies, two other studies failed to find baseline differences in metabolites between converters and non-converters [63, 168]. Both these studies measured metabolites in the PCC. One showed that the future decline in cognitive function among MCI patients was predicted by measurement of absolute quantification of NAA and Cr concentrations [168]. The other study later proposed additionally that NAA/Cr ratio measurement improves the prediction of conversion when added to hippocampal volume measurement [169].

A study of 53 aMCI patients followed for a mean period of 3 years [165] examined by 1.5 T MR scanner using PRESS sequence (TR/TE = 2500/30) demonstrated that the ratio of NAA/Cr in the left occipital cortex predicted progression to dementia at 100% sensitivity and 46% specificity, with an area under the receiver operating characteristic (ROC) curve of 0.69 when thresholding the ratio at or below 1.61. In the

hippocampus, a mIns/Cr ratio higher than 1.04 predicted conversion with 66.7% sensitivity and 72% specificity, with an area under the curve of 0.66. The same author [164] later reported the results of a study of 78 aMCI patients with a mean follow-up period of 2 years. An NAA/Cr ratio equal to or lower than 1.43 in the PCC predicted conversion to AD with 74.1% sensitivity and 83.7% specificity, with an area under the curve of 0.84. In the left medial occipital lobe, the predictive value was somewhat lower, with 85.2% sensitivity and 61.4% specificity, and an area under the curve was 0.8. In another study, of a cohort of 119 consecutive aMCI patients followed for a mean period of 29 months [163] examined by 1.5 T MR machine using PRESS sequence (TR/TE = 2500/30), MRS of the PCC predicted conversion from aMCI to probable AD with 82% sensitivity and 72% specificity, based on an NAA/Cr ratio less than 1.40. Similarly, a mIns/NAA ratio in the PCC higher than 0.47 predicted conversion with 79% sensitivity and 67% specificity, with an area under the curve of 0.77. MRS in the left occipital cortex predicted conversion from aMCI to AD with 78% sensitivity and 69% specificity, with an area under the curve of 0.79 using a NAA/Cr threshold less than 1.57. In a study of 41 aMCI patients and 35 cognitively unimpaired controls with a relatively short follow-up period of 1 year [170], examined by 1.5 T MR scanner using PRESS sequence (TR/TE = 1500/35), the NAA/Cr ratio in the left hippocampus was significantly lower in aMCI patients than in controls ($p = 0.008$), but there were no differences in metabolite ratios at baseline between aMCI converters and stable subjects. A mIns/Cr ratio of 0.349 or more in the right parietal lobe predicted progression of disease with 70% sensitivity and 85% specificity. Unfortunately there are no studies reporting absolute values of metabolites.

One interesting project sought surrogate markers for development of MCI using quantitative MRI and MRS markers [171]. Subjects were recruited from cognitively normal 1156 subjects in the population-based Mayo Clinic Study and underwent MRI and MRS examinations. MRS focused on the PCC, and volumes of hippocampus and white matter hyperintensity were measured automatically. After a median follow-up of 2.8 years, 214 subjects had progressed to MCI or dementia. In multivariable modeling, only decreased hippocampal volume and NAA/mIns in the PCC were independent predictors of MCI, with hazard ratio of 1.8 and 1.4, respectively.

To summarize, MRS shows promising results for predicting conversion from MCI to AD, but it is not currently proven by measuring absolute values. The use of absolute quantification, rather than metabolite ratios, may improve the reliability of MRS for this purpose. For earlier diagnosis of MCI, MRS of the hippocampus and entorhinal cortex may be preferable, but MRS of these regions is technically more difficult because of small volumes, field inhomogeneities due to air sinuses, and the presence of cerebrospinal fluid.

7.7.4 Limits on Progress

The technical/procedural aspects of proton MRS have improved with time, but clinical applications have not kept pace. There are as yet insufficient MRS data on the significance of metabolite changes found with various pathological processes. Also,

lack of consensus on standard procedures for MRS complicates the interpretation of results, especially for the purposes of multicenter analysis, which in turn creates difficulty for clinical application of MRS to dementia diagnosis.

References

1. Klunk WE, Panchalingam K, Moossy J, McClure RJ, Pettegrew JW. N-acetyl-L-aspartate and other amino acid metabolites in Alzheimer's disease brain: a preliminary proton nuclear magnetic resonance study. Neurology. 1992;42(8):1578–85.
2. Shiino A, Matsuda M, Morikawa S, Inubushi T, Akiguchi I, Handa J. Proton magnetic resonance spectroscopy with dementia. Surg Neurol. 1993;39(2):143–7.
3. Miller BL, Moats RA, Shonk T, Ernst T, Woolley S, Ross BD. Alzheimer disease: depiction of increased cerebral myo-inositol with proton MR spectroscopy. Radiology. 1993;187(2):433–7. doi:10.1148/radiology.187.2.8475286.
4. Drost DJ, Riddle WR, Clarke GD, Group AMT. Proton magnetic resonance spectroscopy in the brain: report of AAPM MR Task Group #9. Med Phys. 2002;29(9):2177–97.
5. Mekle R, Mlynarik V, Gambarota G, Hergt M, Krueger G, Gruetter R. MR spectroscopy of the human brain with enhanced signal intensity at ultrashort echo times on a clinical platform at 3T and 7T. Magn Reson Med. 2009;61(6):1279–85. doi:10.1002/mrm.21961.
6. Duarte JM, Lei H, Mlynarik V, Gruetter R. The neurochemical profile quantified by in vivo 1H NMR spectroscopy. NeuroImage. 2012;61(2):342–62. doi:10.1016/j.neuroimage.2011.12.038.
7. O'Gorman RL, Michels L, Edden RA, Murdoch JB, Martin E. In vivo detection of GABA and glutamate with MEGA-PRESS: reproducibility and gender effects. J Magn Reson Imaging. 2011;33(5):1262–7. doi:10.1002/jmri.22520.
8. Birken DL, Oldendorf WH. N-acetyl-L-aspartic acid: a literature review of a compound prominent in 1H-NMR spectroscopic studies of brain. Neurosci Biobehav Rev. 1989;13(1):23–31.
9. Burri R, Bigler P, Straehl P, Posse S, Colombo JP, Herschkowitz N. Brain development: 1H magnetic resonance spectroscopy of rat brain extracts compared with chromatographic methods. Neurochem Res. 1990;15(10):1009–16.
10. Nadler JV, Cooper JR. N-acetyl-L-aspartic acid content of human neural tumours and bovine peripheral nervous tissues. J Neurochem. 1972;19(2):313–9.
11. Miyake M, Kakimoto Y, Sorimachi M. A gas chromatographic method for the determination of N-acetyl-L-aspartic acid, N-acetyl-alpha-aspartylglutamic acid and beta-citryl-L-glutamic acid and their distributions in the brain and other organs of various species of animals. J Neurochem. 1981;36(3):804–10.
12. Ory-Lavollee L, Blakely RD, Coyle JT. Neurochemical and immunocytochemical studies on the distribution of N-acetyl-aspartylglutamate and N-acetyl-aspartate in rat spinal cord and some peripheral nervous tissues. J Neurochem. 1987;48(3):895–9.
13. Baslow MH, Hrabe J, Guilfoyle DN. Dynamic relationship between neurostimulation and N-acetylaspartate metabolism in the human visual cortex: evidence that NAA functions as a molecular water pump during visual stimulation. J Mol Neurosci. 2007;32(3):235–45.
14. Ariyannur PS, Moffett JR, Manickam P, Pattabiraman N, Arun P, Nitta A, Nabeshima T, Madhavarao CN, Namboodiri AM. Methamphetamine-induced neuronal protein NAT8L is the NAA biosynthetic enzyme: implications for specialized acetyl coenzyme A metabolism in the CNS. Brain Res. 2010;1335:1–13. doi:10.1016/j.brainres.2010.04.008.
15. Kreis R, Hofmann L, Kuhlmann B, Boesch C, Bossi E, Huppi PS. Brain metabolite composition during early human brain development as measured by quantitative in vivo 1H magnetic resonance spectroscopy. Magn Reson Med. 2002;48(6):949–58. doi:10.1002/mrm.10304.
16. Pouwels PJ, Brockmann K, Kruse B, Wilken B, Wick M, Hanefeld F, Frahm J. Regional age dependence of human brain metabolites from infancy to adulthood as detected by quantitative localized proton MRS. Pediatr Res. 1999;46(4):474–85. doi:10.1203/00006450-199910000-00019.

17. Urenjak J, Williams SR, Gadian DG, Noble M. Specific expression of N-acetylaspartate in neurons, oligodendrocyte-type-2 astrocyte progenitors, and immature oligodendrocytes in vitro. J Neurochem. 1992;59(1):55–61.
18. Baslow MH. N-acetylaspartate in the vertebrate brain: metabolism and function. Neurochem Res. 2003;28(6):941–53.
19. Baslow MH. N-acetylaspartate and N-acetylaspartylglutamate. In: Lajtha A, Oja S, Schousboe A, Saransaari P, editors. Handbook of neurochemistry and molecular neurobiology: amino acids and peptides in the nervous system. New York: Springer; 2007. p. 305–46.
20. Choi IY, Gruetter R. In vivo 13C NMR assessment of brain glycogen concentration and turnover in the awake rat. Neurochem Int. 2003;43(4-5):317–22.
21. Choi IY, Gruetter R. Dynamic or inert metabolism? Turnover of N-acetyl aspartate and glutathione from D-[1-13C]glucose in the rat brain in vivo. J Neurochem. 2004;91(4):778–87. doi:10.1111/j.1471-4159.2004.02716.x.
22. Moreno A, Ross BD, Bluml S. Direct determination of the N-acetyl-L-aspartate synthesis rate in the human brain by (13)C MRS and [1-(13)C]glucose infusion. J Neurochem. 2001;77(1):347–50.
23. Hyder F, Chase JR, Behar KL, Mason GF, Siddeek M, Rothman DL, Shulman RG. Increased tricarboxylic acid cycle flux in rat brain during forepaw stimulation detected with 1H[13C] NMR. Proc Natl Acad Sci U S A. 1996;93(15):7612–7.
24. Pfeuffer J, Tkac I, Choi IY, Merkle H, Ugurbil K, Garwood M, Gruetter R. Localized in vivo 1H NMR detection of neurotransmitter labeling in rat brain during infusion of [1-13C] D-glucose. Magn Reson Med. 1999;41(6):1077–83.
25. Pfeuffer J, Tkac I, Provencher SW, Gruetter R. Toward an in vivo neurochemical profile: quantification of 18 metabolites in short-echo-time (1)H NMR spectra of the rat brain. J Magn Reson. 1999;141(1):104–20. doi:10.1006/jmre.1999.1895.
26. Wiame E, Tyteca D, Pierrot N, Collard F, Amyere M, Noel G, Desmedt J, Nassogne MC, Vikkula M, Octave JN, Vincent MF, Courtoy PJ, Boltshauser E, van Schaftingen E. Molecular identification of aspartate N-acetyltransferase and its mutation in hypoacetylaspartia. Biochem J. 2010;425(1):127–36. doi:10.1042/BJ20091024.
27. Tahay G, Wiame E, Tyteca D, Courtoy PJ, Van Schaftingen E. Determinants of the enzymatic activity and the subcellular localization of aspartate N-acetyltransferase. Biochem J. 2012;441(1):105–12. doi:10.1042/BJ20111179.
28. Huang W, Wang H, Kekuda R, Fei YJ, Friedrich A, Wang J, Conway SJ, Cameron RS, Leibach FH, Ganapathy V. Transport of N-acetylaspartate by the Na(+)-dependent high-affinity dicarboxylate transporter NaDC3 and its relevance to the expression of the transporter in the brain. J Pharmacol Exp Ther. 2000;295(1):392–403.
29. Burri R, Steffen C, Herschkowitz N. N-acetyl-L-aspartate is a major source of acetyl groups for lipid synthesis during rat brain development. Dev Neurosci. 1991;13(6):403–11.
30. Namboodiri AM, Peethambaran A, Mathew R, Sambhu PA, Hershfield J, Moffett JR, Madhavarao CN. Canavan disease and the role of N-acetylaspartate in myelin synthesis. Mol Cell Endocrinol. 2006;252(1-2):216–23. doi:10.1016/j.mce.2006.03.016.
31. Martin E, Capone A, Schneider J, Hennig J, Thiel T. Absence of N-acetylaspartate in the human brain: impact on neurospectroscopy? Ann Neurol. 2001;49(4):518–21.
32. Boltshauser E, Schmitt B, Wevers RA, Engelke U, Burlina AB, Burlina AP. Follow-up of a child with hypoacetylaspartia. Neuropediatrics. 2004;35(4):255–8. doi:10.1055/s-2004-821036.
33. Burlina AP, Schmitt B, Engelke U, Wevers RA, Burlina AB, Boltshauser E. Hypoacetylaspartia: clinical and biochemical follow-up of a patient. Adv Exp Med Biol. 2006;576:283–287. discussion 361-283. doi:10.1007/0-387-30172-0_20.
34. Becker I, Lodder J, Gieselmann V, Eckhardt M. Molecular characterization of N-acetylaspartylglutamate synthetase. J Biol Chem. 2010;285(38):29156–64. doi:10.1074/jbc.M110.111765.
35. Wroblewska B, Santi MR, Neale JH. N-acetylaspartylglutamate activates cyclic AMP-coupled metabotropic glutamate receptors in cerebellar astrocytes. Glia. 1998;24(2):172–9.

36. Wroblewska B, Wroblewski JT, Saab OH, Neale JH. N-acetylaspartylglutamate inhibits forskolin-stimulated cyclic AMP levels via a metabotropic glutamate receptor in cultured cerebellar granule cells. J Neurochem. 1993;61(3):943–8.
37. Hayashi Y, Momiyama A, Takahashi T, Ohishi H, Ogawa-Meguro R, Shigemoto R, Mizuno N, Nakanishi S. Role of a metabotropic glutamate receptor in synaptic modulation in the accessory olfactory bulb. Nature. 1993;366(6456):687–90. doi:10.1038/366687a0.
38. Sanchez-Prieto J, Budd DC, Herrero I, Vazquez E, Nicholls DG. Presynaptic receptors and the control of glutamate exocytosis. Trends Neurosci. 1996;19(6):235–9.
39. Wroblewska B, Wegorzewska IN, Bzdega T, Olszewski RT, Neale JH. Differential negative coupling of type 3 metabotropic glutamate receptor to cyclic GMP levels in neurons and astrocytes. J Neurochem. 2006;96(4):1071–7. doi:10.1111/j.1471-4159.2005.03569.x.
40. Cartmell J, Schoepp DD. Regulation of neurotransmitter release by metabotropic glutamate receptors. J Neurochem. 2000;75(3):889–907.
41. Gafurov B, Urazaev AK, Grossfeld RM, Lieberman EM. N-acetylaspartylglutamate (NAAG) is the probable mediator of axon-to-glia signaling in the crayfish medial giant nerve fiber. Neuroscience. 2001;106(1):227–35.
42. Mesters JR, Barinka C, Li W, Tsukamoto T, Majer P, Slusher BS, Konvalinka J, Hilgenfeld R. Structure of glutamate carboxypeptidase II, a drug target in neuronal damage and prostate cancer. EMBO J. 2006;25(6):1375–84. doi:10.1038/sj.emboj.7600969.
43. Kaldis P, Hemmer W, Zanolla E, Holtzman D, Wallimann T. 'Hot spots' of creatine kinase localization in brain: cerebellum, hippocampus and choroid plexus. Dev Neurosci. 1996;18(5-6):542–54.
44. Aksenova MV, Burbaeva GS, Kandror KV, Kapkov DV, Stepanov AS. The decreased level of casein kinase 2 in brain cortex of schizophrenic and Alzheimer's disease patients. FEBS Lett. 1991;279(1):55–7.
45. Happe HK, Murrin LC. In situ hybridization analysis of CHOT1, a creatine transporter, in the rat central nervous system. J Comp Neurol. 1995;351(1):94–103. doi:10.1002/cne.903510109.
46. Saltarelli MD, Bauman AL, Moore KR, Bradley CC, Blakely RD. Expression of the rat brain creatine transporter in situ and in transfected HeLa cells. Dev Neurosci. 1996;18(5–6):524–34.
47. Schloss P, Mayser W, Betz H. The putative rat choline transporter CHOT1 transports creatine and is highly expressed in neural and muscle-rich tissues. Biochem Biophys Res Commun. 1994;198(2):637–45. doi:10.1006/bbrc.1994.1093.
48. Braissant O, Henry H, Loup M, Eilers B, Bachmann C. Endogenous synthesis and transport of creatine in the rat brain: an in situ hybridization study. Brain Res Mol Brain Res. 2001;86(1-2):193–201.
49. Ohtsuki S, Tachikawa M, Takanaga H, Shimizu H, Watanabe M, Hosoya K, Terasaki T. The blood-brain barrier creatine transporter is a major pathway for supplying creatine to the brain. J Cereb Blood Flow Metab. 2002;22(11):1327–35. doi:10.1097/00004647-200211000-00006.
50. Perasso L, Cupello A, Lunardi GL, Principato C, Gandolfo C, Balestrino M. Kinetics of creatine in blood and brain after intraperitoneal injection in the rat. Brain Res. 2003;974(1-2):37–42.
51. Braissant O, Bachmann C, Henry H. Expression and function of AGAT, GAMT and CT1 in the mammalian brain. Subcell Biochem. 2007;46:67–81.
52. Braissant O, Henry H. AGAT, GAMT and SLC6A8 distribution in the central nervous system, in relation to creatine deficiency syndromes: a review. J Inherit Metab Dis. 2008;31(2):230–9. doi:10.1007/s10545-008-0826-9.
53. Nakashima T, Tomi M, Tachikawa M, Watanabe M, Terasaki T, Hosoya K. Evidence for creatine biosynthesis in Muller glia. Glia. 2005;52(1):47–52. doi:10.1002/glia.20222.
54. Schmidt A, Marescau B, Boehm EA, Renema WK, Peco R, Das A, Steinfeld R, Chan S, Wallis J, Davidoff M, Ullrich K, Waldschutz R, Heerschap A, De Deyn PP, Neubauer S, Isbrandt D. Severely altered guanidino compound levels, disturbed body weight homeostasis and impaired fertility in a mouse model of guanidinoacetate N-methyltransferase (GAMT) deficiency. Hum Mol Genet. 2004;13(9):905–21. doi:10.1093/hmg/ddh112.

55. Tachikawa M, Fukaya M, Terasaki T, Ohtsuki S, Watanabe M. Distinct cellular expressions of creatine synthetic enzyme GAMT and creatine kinases uCK-Mi and CK-B suggest a novel neuron-glial relationship for brain energy homeostasis. Eur J Neurosci. 2004;20(1):144–60. doi:10.1111/j.1460-9568.2004.03478.x.
56. Salomons GS, van Dooren SJ, Verhoeven NM, Cecil KM, Ball WS, Degrauw TJ, Jakobs C. X-linked creatine-transporter gene (SLC6A8) defect: a new creatine-deficiency syndrome. Am J Hum Genet. 2001;68(6):1497–500. doi:10.1086/320595.
57. Zwaal RF, Comfurius P, Bevers EM. Surface exposure of phosphatidylserine in pathological cells. Cell Mol Life Sci. 2005;62(9):971–88. doi:10.1007/s00018-005-4527-3.
58. Naudi A, Jove M, Ayala V, Cabre R, Portero-Otin M, Pamplona R. Non-enzymatic modification of aminophospholipids by carbonyl-amine reactions. Int J Mol Sci. 2013;14(2):3285–313. doi:10.3390/ijms14023285.
59. Pouwels PJ, Frahm J. Regional metabolite concentrations in human brain as determined by quantitative localized proton MRS. Magn Reson Med. 1998;39(1):53–60.
60. Tan J, Bluml S, Hoang T, Dubowitz D, Mevenkamp G, Ross B. Lack of effect of oral choline supplement on the concentrations of choline metabolites in human brain. Magn Reson Med. 1998;39(6):1005–10.
61. Wang Y, Li SJ. Differentiation of metabolic concentrations between gray matter and white matter of human brain by in vivo 1H magnetic resonance spectroscopy. Magn Reson Med. 1998;39(1):28–33.
62. Bluml S, Seymour KJ, Ross BD. Developmental changes in choline- and ethanolamine-containing compounds measured with proton-decoupled (31)P MRS in in vivo human brain. Magn Reson Med. 1999;42(4):643–54.
63. Kantarci K, Weigand SD, Petersen RC, Boeve BF, Knopman DS, Gunter J, Reyes D, Shiung M, O'Brien PC, Smith GE, Ivnik RJ, Tangalos EG, Jack CR Jr. Longitudinal 1H MRS changes in mild cognitive impairment and Alzheimer's disease. Neurobiol Aging. 2007;28(9):1330–9. doi:10.1016/j.neurobiolaging.2006.06.018.
64. DeKosky ST, Ikonomovic MD, Styren SD, Beckett L, Wisniewski S, Bennett DA, Cochran EJ, Kordower JH, Mufson EJ. Upregulation of choline acetyltransferase activity in hippocampus and frontal cortex of elderly subjects with mild cognitive impairment. Ann Neurol. 2002;51(2):145–55.
65. Ballard C, Gauthier S, Corbett A, Brayne C, Aarsland D, Jones E. Alzheimer's disease. Lancet. 2011;377(9770):1019–31. doi:10.1016/S0140-6736(10)61349-9.
66. Zhang YW, Thompson R, Zhang H, Xu H. APP processing in Alzheimer's disease. Mol Brain. 2011;4:3. doi:10.1186/1756-6606-4-3.
67. Gentile MT, Reccia MG, Sorrentino PP, Vitale E, Sorrentino G, Puca AA, Colucci-D'Amato L. Role of cytosolic calcium-dependent phospholipase A2 in Alzheimer's disease pathogenesis. Mol Neurobiol. 2012;45(3):596–604. doi:10.1007/s12035-012-8279-4.
68. Kwon HM, Yamauchi A, Uchida S, Preston AS, Garcia-Perez A, Burg MB, Handler JS. Cloning of the cDNa for a Na+/myo-inositol cotransporter, a hypertonicity stress protein. J Biol Chem. 1992;267(9):6297–301.
69. Paredes A, McManus M, Kwon HM, Strange K. Osmoregulation of Na(+)-inositol cotransporter activity and mRNA levels in brain glial cells. Am J Phys. 1992;263(6 Pt 1):C1282–8.
70. Fisher SK, Novak JE, Agranoff BW. Inositol and higher inositol phosphates in neural tissues: homeostasis, metabolism and functional significance. J Neurochem. 2002;82(4):736–54.
71. Bissonnette P, Lahjouji K, Coady MJ, Lapointe JY. Effects of hyperosmolarity on the Na+-myo-inositol cotransporter SMIT2 stably transfected in the Madin-Darby canine kidney cell line. Am J Physiol Cell Physiol. 2008;295(3):C791–9. doi:10.1152/ajpcell.00390.2007.
72. Ibsen L, Strange K. In situ localization and osmotic regulation of the Na(+)-myo-inositol cotransporter in rat brain. Am J Phys. 1996;271(4 Pt 2):F877–85.
73. Isaacks RE, Bender AS, Kim CY, Prieto NM, Norenberg MD. Osmotic regulation of myo-inositol uptake in primary astrocyte cultures. Neurochem Res. 1994;19(3):331–8.

74. Klaus F, Palmada M, Lindner R, Laufer J, Jeyaraj S, Lang F, Boehmer C. Up-regulation of hypertonicity-activated myo-inositol transporter SMIT1 by the cell volume-sensitive protein kinase SGK1. J Physiol. 2008;586(6):1539–47. doi:10.1113/jphysiol.2007.146191.
75. Wiese TJ, Dunlap JA, Conner CE, Grzybowski JA, Lowe WL Jr, Yorek MA. Osmotic regulation of Na-myo-inositol cotransporter mRNA level and activity in endothelial and neural cells. Am J Phys. 1996;270(4 Pt 1):C990–7.
76. Uldry M, Ibberson M, Horisberger JD, Chatton JY, Riederer BM, Thorens B. Identification of a mammalian H(+)-myo-inositol symporter expressed predominantly in the brain. EMBO J. 2001;20(16):4467–77. doi:10.1093/emboj/20.16.4467.
77. Di Daniel E, Mok MH, Mead E, Mutinelli C, Zambello E, Caberlotto LL, Pell TJ, Langmead CJ, Shah AJ, Duddy G, Kew JN, Maycox PR. Evaluation of expression and function of the H+/myo-inositol transporter HMIT. BMC Cell Biol. 2009;10:54. doi:10.1186/1471-2121-10-54.
78. Uldry M, Steiner P, Zurich MG, Beguin P, Hirling H, Dolci W, Thorens B. Regulated exocytosis of an H+/myo-inositol symporter at synapses and growth cones. EMBO J. 2004;23(3):531–40. doi:10.1038/sj.emboj.7600072.
79. Augustin R. The protein family of glucose transport facilitators: it's not only about glucose after all. IUBMB Life. 2010;62(5):315–33. doi:10.1002/iub.315.
80. Fu H, Li B, Hertz L, Peng L. Contributions in astrocytes of SMIT1/2 and HMIT to myo-inositol uptake at different concentrations and pH. Neurochem Int. 2012;61(2):187–94. doi:10.1016/j.neuint.2012.04.010.
81. Sturrock A, Laule C, Decolongon J, Dar Santos R, Coleman AJ, Creighton S, Bechtel N, Reilmann R, Hayden MR, Tabrizi SJ, Mackay AL, Leavitt BR. Magnetic resonance spectroscopy biomarkers in premanifest and early Huntington disease. Neurology. 2010;75(19):1702–10. doi:10.1212/WNL.0b013e3181fc27e4.
82. Oz G, Hutter D, Tkac I, Clark HB, Gross MD, Jiang H, Eberly LE, Bushara KO, Gomez CM. Neurochemical alterations in spinocerebellar ataxia type 1 and their correlations with clinical status. Mov Disord. 2010;25(9):1253–61. doi:10.1002/mds.23067.
83. Huang W, Alexander GE, Daly EM, Shetty HU, Krasuski JS, Rapoport SI, Schapiro MB. High brain myo-inositol levels in the predementia phase of Alzheimer's disease in adults with Down's syndrome: a 1H MRS study. Am J Psychiatry. 1999;156(12):1879–86.
84. Beacher F, Simmons A, Daly E, Prasher V, Adams C, Margallo-Lana ML, Morris R, Lovestone S, Murphy K, Murphy DG. Hippocampal myo-inositol and cognitive ability in adults with Down syndrome: an in vivo proton magnetic resonance spectroscopy study. Arch Gen Psychiatry. 2005;62(12):1360–5. doi:10.1001/archpsyc.62.12.1360.
85. Lamar M, Foy CM, Beacher F, Daly E, Poppe M, Archer N, Prasher V, Murphy KC, Morris RG, Simmons A, Lovestone S, Murphy DG. Down syndrome with and without dementia: an in vivo proton magnetic resonance spectroscopy study with implications for Alzheimer's disease. NeuroImage. 2011;57(1):63–8. doi:10.1016/j.neuroimage.2011.03.073.
86. Berry GT, Mallee JJ, Kwon HM, Rim JS, Mulla WR, Muenke M, Spinner NB. The human osmoregulatory Na+/myo-inositol cotransporter gene (SLC5A3): molecular cloning and localization to chromosome 21. Genomics. 1995;25(2):507–13.
87. Videen JS, Michaelis T, Pinto P, Ross BD. Human cerebral osmolytes during chronic hyponatremia. A proton magnetic resonance spectroscopy study. J Clin Invest. 1995;95(2):788–93. doi:10.1172/JCI117728.
88. Lien YH, Shapiro JI, Chan L. Effects of hypernatremia on organic brain osmoles. J Clin Invest. 1990;85(5):1427–35. doi:10.1172/JCI114587.
89. Brusilow SW, Koehler RC, Traystman RJ, Cooper AJ. Astrocyte glutamine synthetase: importance in hyperammonemic syndromes and potential target for therapy. Neurotherapeutics. 2010;7(4):452–70. doi:10.1016/j.nurt.2010.05.015.
90. Davanzo P, Thomas MA, Yue K, Oshiro T, Belin T, Strober M, McCracken J. Decreased anterior cingulate myo-inositol/creatine spectroscopy resonance with lithium treatment in children with bipolar disorder. Neuropsychopharmacology. 2001;24(4):359–69. doi:10.1016/S0893-133X(00)00207-4.

91. Moore GJ, Bebchuk JM, Parrish JK, Faulk MW, Arfken CL, Strahl-Bevacqua J, Manji HK. Temporal dissociation between lithium-induced changes in frontal lobe myo-inositol and clinical response in manic-depressive illness. Am J Psychiatry. 1999;156(12):1902–8.
92. Shaltiel G, Shamir A, Shapiro J, Ding D, Dalton E, Bialer M, Harwood AJ, Belmaker RH, Greenberg ML, Agam G. Valproate decreases inositol biosynthesis. Biol Psychiatry. 2004;56(11):868–74. doi:10.1016/j.biopsych.2004.08.027.
93. Williams RS, Harwood AJ. Lithium therapy and signal transduction. Trends Pharmacol Sci. 2000;21(2):61–4.
94. Brand A, Richter-Landsberg C, Leibfritz D. Multinuclear NMR studies on the energy metabolism of glial and neuronal cells. Dev Neurosci. 1993;15(3-5):289–98.
95. Glanville NT, Byers DM, Cook HW, Spence MW, Palmer FB. Differences in the metabolism of inositol and phosphoinositides by cultured cells of neuronal and glial origin. Biochim Biophys Acta. 1989;1004(2):169–79.
96. Duarte JM, Carvalho RA, Cunha RA, Gruetter R. Caffeine consumption attenuates neurochemical modifications in the hippocampus of streptozotocin-induced diabetic rats. J Neurochem. 2009;111(2):368–79. doi:10.1111/j.1471-4159.2009.06349.x.
97. Kim JP, Lentz MR, Westmoreland SV, Greco JB, Ratai EM, Halpern E, Lackner AA, Masliah E, Gonzalez RG. Relationships between astrogliosis and 1H MR spectroscopic measures of brain choline/creatine and myo-inositol/creatine in a primate model. AJNR Am J Neuroradiol. 2005;26(4):752–9.
98. Kunz N, Camm EJ, Somm E, Lodygensky G, Darbre S, Aubert ML, Huppi PS, Sizonenko SV, Gruetter R. Developmental and metabolic brain alterations in rats exposed to bisphenol A during gestation and lactation. Int J Dev Neurosci. 2011;29(1):37–43. doi:10.1016/j.ijdevneu.2010.09.009.
99. Godfrey DA, Hallcher LM, Laird MH, Matschinsky FM, Sherman WR. Distribution of myo-inositol in the cat cochlear nucleus. J Neurochem. 1982;38(4):939–47.
100. Sherman WR, Packman PM, Laird MH, Boshans RL. Measurement of myo-inositol in single cells and defined areas of the nervous system by selected ion monitoring. Anal Biochem. 1977;78(1):119–31.
101. Hertz L, Peng L, Dienel GA. Energy metabolism in astrocytes: high rate of oxidative metabolism and spatiotemporal dependence on glycolysis/glycogenolysis. J Cereb Blood Flow Metab. 2007;27(2):219–49. doi:10.1038/sj.jcbfm.9600343.
102. Shen J, Petersen KF, Behar KL, Brown P, Nixon TW, Mason GF, Petroff OA, Shulman GI, Shulman RG, Rothman DL. Determination of the rate of the glutamate/glutamine cycle in the human brain by in vivo 13C NMR. Proc Natl Acad Sci U S A. 1999;96(14):8235–40.
103. Waagepetersen HS, Sonnewald U, Schousboe A. Glutamine, glutamate, and GABA: metabolic aspects. In: Lajtha A, Oja S, Schousboe A, Saransaari P, editors. Handbook of neurochemistry and molecular neurobiology: amino acids and peptides in the nervous system. New York: Springer; 2007. p. 1–21.
104. Govindaraju V, Young K, Maudsley AA. Proton NMR chemical shifts and coupling constants for brain metabolites. NMR Biomed. 2000;13(3):129–53.
105. Jensen JE, Licata SC, Ongur D, Friedman SD, Prescot AP, Henry ME, Renshaw PF. Quantification of J-resolved proton spectra in two-dimensions with LCModel using GAMMA-simulated basis sets at 4 Tesla. NMR Biomed. 2009;22(7):762–9. doi:10.1002/nbm.1390.
106. Kauppinen RA, Williams SR. Nondestructive detection of glutamate by 1H nuclear magnetic resonance spectroscopy in cortical brain slices from the guinea pig: evidence for changes in detectability during severe anoxic insults. J Neurochem. 1991;57(4):1136–44.
107. Bartha R, Drost DJ, Menon RS, Williamson PC. Spectroscopic lineshape correction by QUECC: combined QUALITY deconvolution and eddy current correction. Magn Reson Med. 2000;44(4):641–5.
108. Dong Z, Peterson BS. Spectral resolution amelioration by deconvolution (SPREAD) in MR spectroscopic imaging. J Magn Reson Imaging. 2009;29(6):1395–405. doi:10.1002/jmri.21784.

109. Poullet JB, Sima DM, Simonetti AW, De Neuter B, Vanhamme L, Lemmerling P, Van Huffel S. An automated quantitation of short echo time MRS spectra in an open source software environment: AQSES. NMR Biomed. 2007;20(5):493–504. doi:10.1002/nbm.1112.
110. Provencher SW. Automatic quantitation of localized in vivo 1H spectra with LCModel. NMR Biomed. 2001;14(4):260–4.
111. Slotboom J, Boesch C, Kreis R. Versatile frequency domain fitting using time domain models and prior knowledge. Magn Reson Med. 1998;39(6):899–911.
112. Sima DM, Osorio-Garcia MI, Poullet J-B, Suvichakorn A, Antoine J-P, Van Huffel S, van Ormondt D. Lineshape estimation for MRS signals: self-deconvolution revisited. Meas Sci Technol. 2009;20(10):104031. doi:10.1088/0957-0233/20/10/104031.
113. Cudalbu C, Mlynarik V, Gruetter R. Handling macromolecule signals in the quantification of the neurochemical profile. J Alzheimer's Dis. 2012;31(Suppl 3):S101–15. doi:10.3233/JAD-2012-120100.
114. Seeger U, Klose U, Mader I, Grodd W, Nagele T. Parameterized evaluation of macromolecules and lipids in proton MR spectroscopy of brain diseases. Magn Reson Med. 2003;49(1):19–28. doi:10.1002/mrm.10332.
115. Vanhamme L, Sundin T, Van Hecke P, Van Huffel S, Pintelon R. Frequency-selective quantification of biomedical magnetic resonance spectroscopy data. J Magn Reson. 2000;143(1):1–16. doi:10.1006/jmre.1999.1960.
116. Ratiney H, Sdika M, Coenradie Y, Cavassila S, van Ormondt D, Graveron-Demilly D. Time-domain semi-parametric estimation based on a metabolite basis set. NMR Biomed. 2005;18(1):1–13. doi:10.1002/nbm.895.
117. Smith SA, Levante TO, Meier BH, Ernst RR. Computer simulations in magnetic resonance. An object oriented programming approach. J Magn Reson A. 1994;106(1):75–105. doi:10.1006/jmra.1994.1008.
118. De Neuter B, Luts J, Vanhamme L, Lemmerling P, Van Huffel S. Java-based framework for processing and displaying short-echo-time magnetic resonance spectroscopy signals. Comput Methods Prog Biomed. 2007;85(2):129–37. doi:10.1016/j.cmpb.2006.09.005.
119. Poullet JB, Sima DM, Van Huffel S. MRS signal quantitation: a review of time- and frequency-domain methods. J Magn Reson. 2008;195(2):134–44. doi:10.1016/j.jmr.2008.09.005.
120. Poullet JB, Pintelon R, Van Huffel S. A new FIR filter technique for solvent suppression in MRS signals. J Magn Reson. 2009;196(1):61–73. doi:10.1016/j.jmr.2008.10.011.
121. Stefan D, Di Cesare F, Andrasescu A, Popa E, Lazariev A, Vescovo E, Strbak O, Williams S, Starcuk Z, Cabanas M, van Ormondt D, Graveron-Demilly D. Quantitation of magnetic resonance spectroscopy signals: the jMRUI software package. Meas Sci Technol. 2009;20(10):104035. doi:10.1088/0957-0233/20/10/104035.
122. Naressi A, Couturier C, Devos JM, Janssen M, Mangeat C, de Beer R, Graveron-Demilly D. Java-based graphical user interface for the MRUI quantitation package. MAGMA. 2001;12(2-3):141–52.
123. Vanhamme L, van den Boogaart A, Van Huffel S. Improved method for accurate and efficient quantification of MRS data with use of prior knowledge. J Magn Reson. 1997;129(1):35–43.
124. Provencher SW. Estimation of metabolite concentrations from localized in vivo proton NMR spectra. Magn Reson Med. 1993;30(6):672–9.
125. Mosconi E, Sima DM, Osorio Garcia MI, Fontanella M, Fiorini S, Van Huffel S, Marzola P. Different quantification algorithms may lead to different results: a comparison using proton MRS lipid signals. NMR Biomed. 2014;27(4):431–43. doi:10.1002/nbm.3079.
126. Cavassila S, Deval S, Huegen C, van Ormondt D, Graveron-Demilly D. Cramer-Rao bounds: an evaluation tool for quantitation. NMR Biomed. 2001;14(4):278–83.
127. Kreis R. Issues of spectral quality in clinical 1H-magnetic resonance spectroscopy and a gallery of artifacts. NMR Biomed. 2004;17(6):361–81. doi:10.1002/nbm.891.
128. Osorio-Garcia MI. Quantification of magnetic resonance spectroscopy signals with lineshape estimation. J Chemom. 2011;25(4):183–92. doi:10.1002/cem. 1353.

129. Moonen CT, von Kienlin M, van Zijl PC, Cohen J, Gillen J, Daly P, Wolf G. Comparison of single-shot localization methods (STEAM and PRESS) for in vivo proton NMR spectroscopy. NMR Biomed. 1989;2(5-6):201–8.
130. Kwock L. Clinical proton magnetic resonance spectroscopy: basic principles. In: Mukherji SK, editor. Clinical applications of MR spectroscopy. New York: Wiley-Liss; 1998. p. 1–31.
131. Jansen JF, Backes WH, Nicolay K, Kooi ME. 1H MR spectroscopy of the brain: absolute quantification of metabolites. Radiology. 2006;240(2):318–32. doi:10.1148/radiol.2402050314.
132. Brooks JC, Roberts N, Kemp GJ, Gosney MA, Lye M, Whitehouse GH. A proton magnetic resonance spectroscopy study of age-related changes in frontal lobe metabolite concentrations. Cereb Cortex. 2001;11(7):598–605.
133. Sailasuta N, Ernst T, Chang L. Regional variations and the effects of age and gender on glutamate concentrations in the human brain. Magn Reson Imaging. 2008;26(5):667–75. doi:10.1016/j.mri.2007.06.007.
134. Chang L, Jiang CS, Ernst T. Effects of age and sex on brain glutamate and other metabolites. Magn Reson Imaging. 2009;27(1):142–5. doi:10.1016/j.mri.2008.06.002.
135. Charlton RA, McIntyre DJ, Howe FA, Morris RG, Markus HS. The relationship between white matter brain metabolites and cognition in normal aging: the GENIE study. Brain Res. 2007;1164:108–16. doi:10.1016/j.brainres.2007.06.027.
136. Raininko R, Mattsson P. Metabolite concentrations in supraventricular white matter from teenage to early old age: a short echo time 1H magnetic resonance spectroscopy (MRS) study. Acta Radiol. 2010;51(3):309–15. doi:10.3109/02841850903476564.
137. Kantarci K, Weigand SD, Przybelski SA, Preboske GM, Pankratz VS, Vemuri P, Senjem ML, Murphy MC, Gunter JL, Machulda MM, Ivnik RJ, Roberts RO, Boeve BF, Rocca WA, Knopman DS, Petersen RC, Jack CR Jr. MRI and MRS predictors of mild cognitive impairment in a population-based sample. Neurology. 2013;81(2):126–33. doi:10.1212/WNL.0b013e31829a3329.
138. Parnetti L, Tarducci R, Presciutti O, Lowenthal DT, Pippi M, Palumbo B, Gobbi G, Pelliccioli GP, Senin U. Proton magnetic resonance spectroscopy can differentiate Alzheimer's disease from normal aging. Mech Ageing Dev. 1997;97(1):9–14.
139. Rose SE, de Zubicaray GI, Wang D, Galloway GJ, Chalk JB, Eagle SC, Semple J, Doddrell DM. A 1H MRS study of probable Alzheimer's disease and normal aging: implications for longitudinal monitoring of dementia progression. Magn Reson Imaging. 1999;17(2):291–9.
140. Zhu X, Schuff N, Kornak J, Soher B, Yaffe K, Kramer JH, Ezekiel F, Miller BL, Jagust WJ, Weiner MW. Effects of Alzheimer disease on fronto-parietal brain N-acetyl aspartate and myo-inositol using magnetic resonance spectroscopic imaging. Alzheimer Dis Assoc Disord. 2006;20(2):77–85. doi:10.1097/01.wad.0000213809.12553.fc.
141. Kantarci K, Knopman DS, Dickson DW, Parisi JE, Whitwell JL, Weigand SD, Josephs KA, Boeve BF, Petersen RC, Jack CR Jr. Alzheimer disease: postmortem neuropathologic correlates of antemortem 1H MR spectroscopy metabolite measurements. Radiology. 2008;248(1):210–20. doi:10.1148/radiol.2481071590.
142. Jessen F, Block W, Traber F, Keller E, Flacke S, Lamerichs R, Schild HH, Heun R. Decrease of N-acetylaspartate in the MTL correlates with cognitive decline of AD patients. Neurology. 2001;57(5):930–2.
143. Doraiswamy PM, Steffens DC, Pitchumoni S, Tabrizi S. Early recognition of Alzheimer's disease: what is consensual? What is controversial? What is practical? J Clin Psychiatry. 1998;59(Suppl 13):6–18.
144. Murray ME, Przybelski SA, Lesnick TG, Liesinger AM, Spychalla A, Zhang B, Gunter JL, Parisi JE, Boeve BF, Knopman DS, Petersen RC, Jack CR Jr, Dickson DW, Kantarci K. Early Alzheimer's disease neuropathology detected by proton MR spectroscopy. J Neurosci. 2014;34(49):16247–55. doi:10.1523/JNEUROSCI.2027-14.2014.
145. Westman E, Wahlund LO, Foy C, Poppe M, Cooper A, Murphy D, Spenger C, Lovestone S, Simmons A. Combining MRI and MRS to distinguish between Alzheimer's disease and healthy controls. J Alzheimer's Dis. 2010;22(1):171–81. doi:10.3233/JAD-2010-100168.

146. Kantarci K, Xu Y, Shiung MM, O'Brien PC, Cha RH, Smith GE, Ivnik RJ, Boeve BF, Edland SD, Kokmen E, Tangalos EG, Petersen RC, Jack CR Jr. Comparative diagnostic utility of different MR modalities in mild cognitive impairment and Alzheimer's disease. Dement Geriatr Cogn Disord. 2002;14(4):198–207. doi: 66021
147. MacKay S, Ezekiel F, Di Sclafani V, Meyerhoff DJ, Gerson J, Norman D, Fein G, Weiner MW. Alzheimer disease and subcortical ischemic vascular dementia: evaluation by combining MR imaging segmentation and H-1 MR spectroscopic imaging. Radiology. 1996;198(2):537–45. doi:10.1148/radiology.198.2.8596863.
148. Martinez-Bisbal MC, Arana E, Marti-Bonmati L, Molla E, Celda B. Cognitive impairment: classification by 1H magnetic resonance spectroscopy. Eur J Neurol. 2004;11(3):187–93.
149. Schuff N, Capizzano AA, AT D, Amend DL, O'Neill J, Norman D, Kramer J, Jagust W, Miller B, Wolkowitz OM, Yaffe K, Weiner MW. Selective reduction of N-acetylaspartate in medial temporal and parietal lobes in AD. Neurology. 2002;58(6):928–35.
150. Silveira de Souza A, de Oliveira-Souza R, Moll J, Tovar-Moll F, Andreiuolo PA, Bottino CM. Contribution of 1H spectroscopy to a brief cognitive-functional test battery for the diagnosis of mild Alzheimer's disease. Dement Geriatr Cogn Disord. 2011;32(5):351–61. doi:10.1159/000334656.
151. Watanabe T, Shiino A, Akiguchi I. Absolute quantification in proton magnetic resonance spectroscopy is useful to differentiate amnesic mild cognitive impairment from Alzheimer's disease and healthy aging. Dement Geriatr Cogn Disord. 2010;30(1):71–7. doi:10.1159/000318750.
152. Petersen RC, Doody R, Kurz A, Mohs RC, Morris JC, Rabins PV, Ritchie K, Rossor M, Thal L, Winblad B. Current concepts in mild cognitive impairment. Arch Neurol. 2001;58(12):1985–92.
153. Flicker C, Ferris SH, Reisberg B. Mild cognitive impairment in the elderly: predictors of dementia. Neurology. 1991;41(7):1006–9.
154. Geslani DM, Tierney MC, Herrmann N, Szalai JP. Mild cognitive impairment: an operational definition and its conversion rate to Alzheimer's disease. Dement Geriatr Cogn Disord. 2005;19(5-6):383–9. doi:10.1159/000084709.
155. Luis CA, Barker WW, Loewenstein DA, Crum TA, Rogaeva E, Kawarai T, St George-Hyslop P, Duara R. Conversion to dementia among two groups with cognitive impairment. A preliminary report. Dement Geriatr Cogn Disord. 2004;18(3-4):307–13. doi:10.1159/000080124.
156. Wolf H, Grunwald M, Ecke GM, Zedlick D, Bettin S, Dannenberg C, Dietrich J, Eschrich K, Arendt T, Gertz HJ. The prognosis of mild cognitive impairment in the elderly. J Neural Transm Suppl. 1998;54:31–50.
157. Ingles JL, Fisk JD, Merry HR, Rockwood K. Five-year outcomes for dementia defined solely by neuropsychological test performance. Neuroepidemiology. 2003;22(3):172–8. doi:69891
158. Mitchell AJ, Shiri-Feshki M. Rate of progression of mild cognitive impairment to dementia--meta-analysis of 41 robust inception cohort studies. Acta Psychiatr Scand. 2009;119(4):252–65. doi:10.1111/j.1600-0447.2008.01326.x.
159. Markesbery WR. Neuropathologic alterations in mild cognitive impairment: a review. J Alzheimer's Dis. 2010;19(1):221–8. doi:10.3233/JAD-2010-1220.
160. Chao LL, Schuff N, Kramer JH, AT D, Capizzano AA, O'Neill J, Wolkowitz OM, Jagust WJ, Chui HC, Miller BL, Yaffe K, Weiner MW. Reduced medial temporal lobe N-acetylaspartate in cognitively impaired but nondemented patients. Neurology. 2005;64(2):282–9. doi:10.1212/01.WNL.0000149638.45635.FF.
161. Kantarci K, Jack CR Jr, Xu YC, Campeau NG, O'Brien PC, Smith GE, Ivnik RJ, Boeve BF, Kokmen E, Tangalos EG, Petersen RC. Regional metabolic patterns in mild cognitive impairment and Alzheimer's disease: a 1H MRS study. Neurology. 2000;55(2):210–7.
162. Tumati S, Martens S, Aleman A. Magnetic resonance spectroscopy in mild cognitive impairment: systematic review and meta-analysis. Neurosci Biobehav Rev. 2013;37(10 Pt 2):2571–86. doi:10.1016/j.neubiorev.2013.08.004.
163. Fayed N, Davila J, Oliveros A, Castillo J, Medrano JJ. Utility of different MR modalities in mild cognitive impairment and its use as a predictor of conversion to probable dementia. Acad Radiol. 2008;15(9):1089–98. doi:10.1016/j.acra.2008.04.008.

164. Modrego PJ, Fayed N, Sarasa M. Magnetic resonance spectroscopy in the prediction of early conversion from amnestic mild cognitive impairment to dementia: a prospective cohort study. BMJ Open. 2011;1(1):e000007. doi:10.1136/bmjopen-2010-000007.
165. Modrego PJ, Fayed N, Pina MA. Conversion from mild cognitive impairment to probable Alzheimer's disease predicted by brain magnetic resonance spectroscopy. Am J Psychiatry. 2005;162(4):667–75. doi:10.1176/appi.ajp.162.4.667.
166. Rami L, Gomez-Anson B, Sanchez-Valle R, Bosch B, Monte GC, Llado A, Molinuevo JL. Longitudinal study of amnesic patients at high risk for Alzheimer's disease: clinical, neuropsychological and magnetic resonance spectroscopy features. Dement Geriatr Cogn Disord. 2007;24(5):402–10. doi:10.1159/000109750.
167. Metastasio A, Rinaldi P, Tarducci R, Mariani E, Feliziani FT, Cherubini A, Pelliccioli GP, Gobbi G, Senin U, Mecocci P. Conversion of MCI to dementia: role of proton magnetic resonance spectroscopy. Neurobiol Aging. 2006;27(7):926–32. doi:10.1016/j.neurobiolaging.2005.05.002.
168. Pilatus U, Lais C, Rochmont Adu M, Kratzsch T, Frolich L, Maurer K, Zanella FE, Lanfermann H, Pantel J. Conversion to dementia in mild cognitive impairment is associated with decline of N-actylaspartate and creatine as revealed by magnetic resonance spectroscopy. Psychiatry Res. 2009;173(1):1–7. doi:10.1016/j.pscychresns.2008.07.015.
169. Kantarci K, Weigand SD, Przybelski SA, Shiung MM, Whitwell JL, Negash S, Knopman DS, Boeve BF, O'Brien PC, Petersen RC, Jack CR Jr. Risk of dementia in MCI: combined effect of cerebrovascular disease, volumetric MRI, and 1H MRS. Neurology. 2009;72(17):1519–25. doi:10.1212/WNL.0b013e3181a2e864.
170. Targosz-Gajniak MG, Siuda JS, Wicher MM, Banasik TJ, Bujak MA, Augusciak-Duma AM, Opala G. Magnetic resonance spectroscopy as a predictor of conversion of mild cognitive impairment to dementia. J Neurol Sci. 2013;335(1-2):58–63. doi:10.1016/j.jns.2013.08.023.
171. Kantarci K. Magnetic resonance spectroscopy in common dementias. Neuroimaging Clin N Am. 2013;23(3):393–406. doi:10.1016/j.nic.2012.10.004.
172. Gibellini F, Smith TK. The Kennedy pathway – De novo synthesis of phosphatidylethanolamine and phosphatidylcholine. IUBMB Life. 2010;62(6):414–28. doi:10.1002/iub.337.